INFLUENCE OF INTENSE GROUND MOTION ON P-DELTA EFFECT AMPLIFICATION

BY

LAUREN M SANTULLO

THESIS

Submitted in partial fulfillment of the requirements
for the degree of Master of Science in Civil Engineering
in the Graduate College of the
University of Illinois at Urbana-Champaign, 2018

Urbana, Illinois

Adviser:

Assistant Professor Ahmed Elbanna

Abstract

High intensity ground motion can cause significant deformations, which is the basis for additional second-order responses. This analysis uses two recorded ground motions for historical large earthquakes (Kocaeli and Tohoku), a sinusoidal curve, and a simulated ground motion based on the 1906 San Francisco earthquake. These ground motions are applied to material elastic and material plastic version of two benchmark structures developed for the Los Angeles region and the overturning moment and displacements are recorded. The responses are highly dependent on the ground motions, and there is some amplification due to the second-order analysis. The 20-story benchmark structure had more of a second-order amplification, but the moment amplification was under 10% and the displacement amplification was around 5%.

Acknowledgements

I would like to thank my advisor, Dr. Elbanna, and the UIUC CEE department for their continued support throughout my master's degree and thesis. I would also like to thank the benefactors of the Mete A. Sozen, Burton and Erma Lewis, and Page fellowships for their financial support of my master's degree program.

Table of Contents

CHAPTER 1. INTRODUCTION 1
CHAPTER 2. BACKGROUND (LITERATURE REVIEW) 2
CHAPTER 3. ANALYSIS VERIFICATION 6
CHAPTER 4. HIGH-RISE MODELS 14
CHAPTER 5. RESULTS 20
CHAPTER 6. CONCLUSIONS 50
REFERENCES 51

CHAPTER 1. INTRODUCTION

Earthquakes are a dynamic process that affect structures differently based on a structure's and ground motion's natural periods. For example, one earthquake can affect a shorter, stiffer structure differently than it would affect a taller, more flexible structure. Taller buildings are susceptible to long-period areas of the ground motion, where the peak displacement approaches the maximum ground displacement. In the cases of large earthquakes, such as one expected to affect the Western United States in the future, this displacement can approach 5 meters. Displacing the top of a high-rise structure about 5 meters can cause large second-order effects on the moment and displacement that have not yet been quantified.

This paper aims to assess the significance of including second-order effects by comparing them to first-order effects of a structure subjected to large ground motions from different tectonic regions. The selection of ground motions is a subset of the ground motions used in the nonlinear time history analysis in ASCE 7-16. This standard requires at least 11 ground motion sets to be used from the same tectonic regime, fault distances, and site conditions (ASCE 2016). Because there are not many large earthquakes originating in a particular region, ASCE 7 applies a scaling procedure based on the response amplitude. In this procedure, a period range of interest from twice the first natural period to the period corresponding with over 90% modal mass participation is established. Each ground motion pair is scaled by the same constant, so the average of all pairs meets or exceeds a target response spectrum, which is based on matching or exceeding the maximum considered earthquake. Although scaling is an important tool to consider several ground motions for a single structure, it was not used in this paper because of the paper's focus on a few large ground motions.

CHAPTER 2. BACKGROUND (LITERATURE REVIEW)

2.1 Simulated Ground Motion

There are not many earthquakes recorded that have had large intensities. To provide more data, earthquake simulation research has become more prevalent. Dynamic analysis focuses on near-fault mechanics to determine the behavior of earthquake rupture, usually through a finite difference or finite element method. Kinematic analysis assumes a certain energy dissipation and considers how that energy would translate to impact certain areas of interest. The simulated earthquake used in this analysis was developed using the kinematic approach affecting the San Francisco area.

To obtain the source model used for the simulated earthquake data, Song et al. attempted to reconcile the different between a geodetic-data-based source model and seismic-data-based source model. This study focused on the San Andreas fault and the 1906 San Francisco earthquake. To study the geodetic data, a projection method was used to expand the available data beyond the previously used, repeated triangular observations in the northern portion of the fault. This expanded the observation points from 37 to 232 and expanded the triangulated network (Song et al., 2008). From the triangulated network and predefined coordinate system, a geodetic displacement field was generated that supported a conclusion that there was a fault slip instead of land sliding. To obtain smooth coseismic data at different locations, the displacement field was linearly inverted and cross-validated with data not used in the estimation. The calculated coseismic slip is shown in Figure 1 in relation to previously defined models.

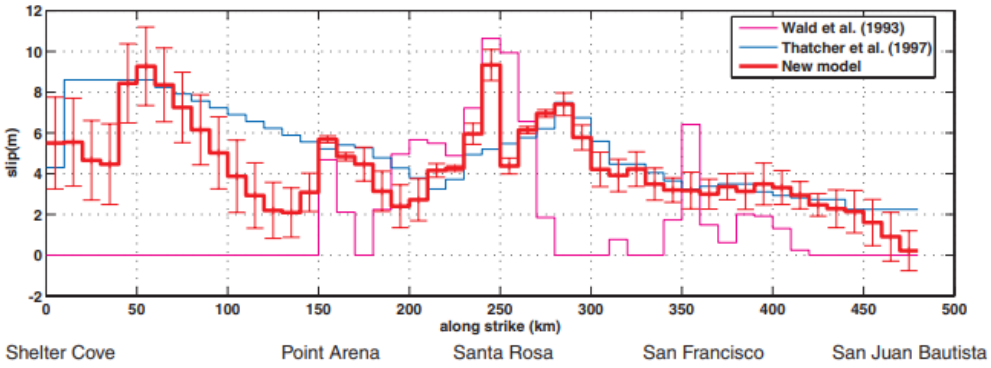

Figure 1: Coseismic Slip Data from Simulated Model (Song et al., 2008)

The Song et al. model also incorporated a study of the 1906 seismic ground motion records available at European, Japanese, and Caribbean stations. Statistical analysis using a Bayesian inversion and Monte Carlo simulation was performed for the slip and rupture velocity. The prior for the velocity used sub-Rayleigh velocity because of its previous use, and the waveforms used were from the 6.2 Morgan Hill earthquake because of similar fault strike in the central portion of the fault. Because the rupture north of the hypocenter was constrained by the European data and the rupture south was constrained by the Caribbean data, a two-segment rupture velocity model was used with a recent prediction of the hypocenter. Combining the seismic and geodetic models, and accounting for rupture velocity above the average shear wave velocity of the Earth's crust, a combined slip model was generated.

The Aagaard et al. analysis uses the Song et al. source model but reduces the average slip for better agreement with other models. Aagaard et al. developed several hypothetical source models based variations of the Song et al. model. These variations included changing the hypocenter location and/or randomizing the slip distribution to account for other possible slip scenarios along the San Andreas fault. The locations of these alternate hypocenters (all at an elevation of -10km) and their relation to urban areas are presented in Figure 2. The modified Song et al. model occurring at Bodega Bay (SongModHypoC) causes ground shaking intensity across the region shown in Figure 3.

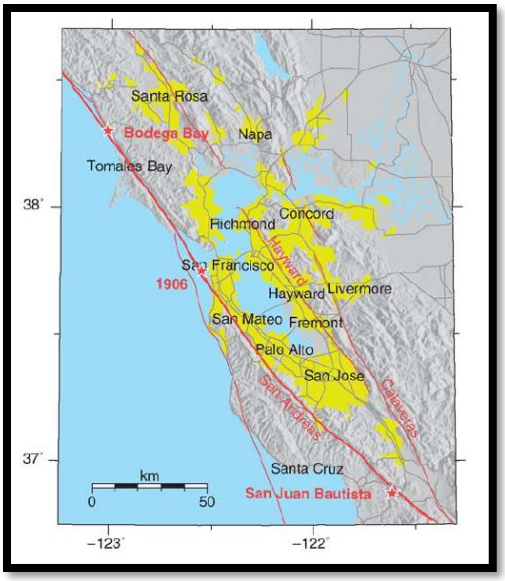

Figure 2: Hypocenter Locations and Urban Areas in the Vicinity of San Francisco (Aagaard et al., 2008)

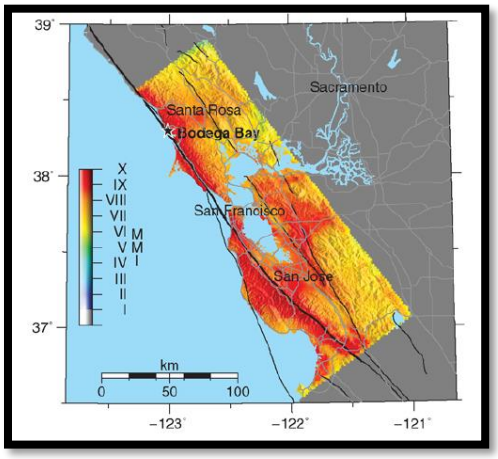

Figure 3: Ground Shaking Intensity due to SongModHypoC (Aagaard et al., 2008)

2.2 Structural Response

The buildings in the San Francisco and Los Angeles urban areas have become taller and more flexible. To better design for these structures, the SAC project worked to develop 3-story, 9-story, and 20-story control benchmark structures. SAC is comprised of the Structural Engineers Association of California (SEAOC), the Applied Technology Council (ATC), and California Universities for research in Earthquake Engineering (CUREE). In contrast to previously published seismically excited benchmark buildings, the ones in Ohtori et al. were designed to behave inelastically. Each structure

has a layout, description of materials used, a frequency plot, and the first three mode shapes provided. (Ohtori et al., 2004).

To simulate material yielding in SAP2000, small plastic hinges are located along members. These are located at points of zero moment that will become hinges once the material yields. For moment frames, where each frame can be compared to a fixed-fixed beam-column member, this is at about 10% of the beam length on each end. SAP2000 uses colors to represent different points of plasticity, shown in Figure 4.

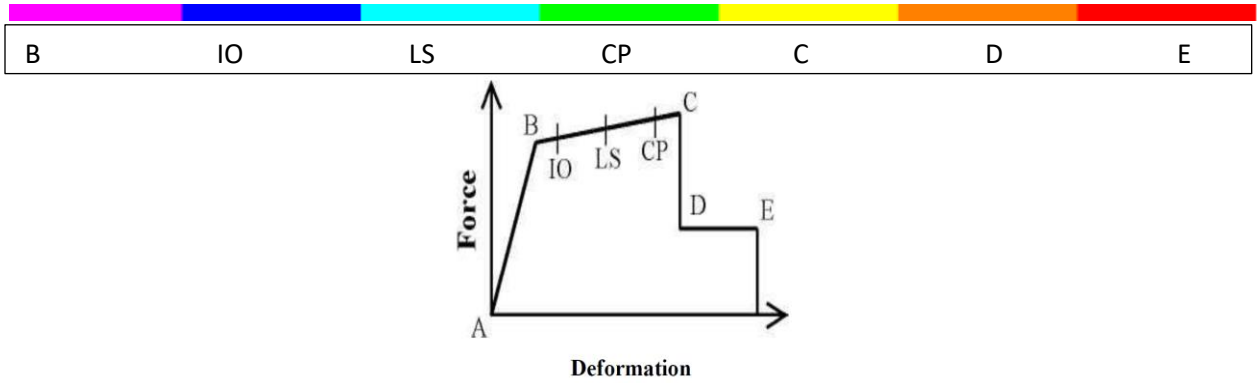

Figure 4: SAP2000 Hinge Response and Corresponding Points on Force-Displacement Diagram (Srinivasu, 2013)

CHAPTER 3. ANALYSIS VERIFICATION

3.1 Single Degree of Freedom Amplification

A high-rise structure, or any dynamically sensitive structure, can be idealized with a point mass and spring system. Converting it to an equivalent single degree of freedom system simplifies the analysis and allows different natural periods to be tested easily. It is relatively simple to change the mass or stiffness and compare the response to the altered natural period. Having only one degree of freedom also clarifies the mode that the response corresponds to. When a structure has multiple modes, the response is due to several primary modes. Although these primary modes are usually related to the highest periods, this is not always the case.

The single degree of freedom model, shown in Figure 5, was used to determine an expected moment amplification value. The first-order and second-order moment relationships in Equations 1 and 2 were based on the Figure 5 geometry. Both moment relationships were based on a quasi-static system, where a lateral force applied could be equated to the spring's force response. The relationship between the natural period, weight, and stiffness was incorporated for Equation 2. The moment amplification factor (Equation 3) we obtained by dividing the second order response by the first order response.

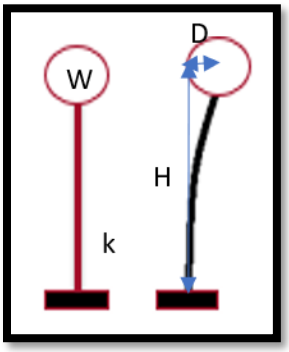

Figure 5: Idealized Single Degree of Freedom System

$$M_1 = kDH \quad \text{(Equation 1)}$$

$$M_2 = kDH + WD \quad \text{(Equation 2)}$$

$$M_2 = kDH\left(1 + \frac{T^2 g}{4\pi^2 H}\right)$$

$$Factor = 1 + \frac{T^2 g}{4\pi^2 H} \quad \text{(Equation 3)}$$

where,

k is the spring stiffness
D is the mass horizontal displacement
H is the height of the spring
W is the weight of the lumped mass
T is the natural period of the system
g is a gravitational acceleration constant
M_1, M_2 are the first-order and second-order moments respectively

This moment amplification is a lower bound estimation based on SAP2000 model results. Various lumped masses and stiffnesses were used to obtain the datapoints in Figure 6 and the calculated period was normalized. To ensure that the entire mass was focused at the top as in Figure 5, weightless steel members of different shapes, and therefore different stiffnesses, acted as the "spring" in the model. Almost all data points lie above the line, representing the moment amplification factor in Equation 3.

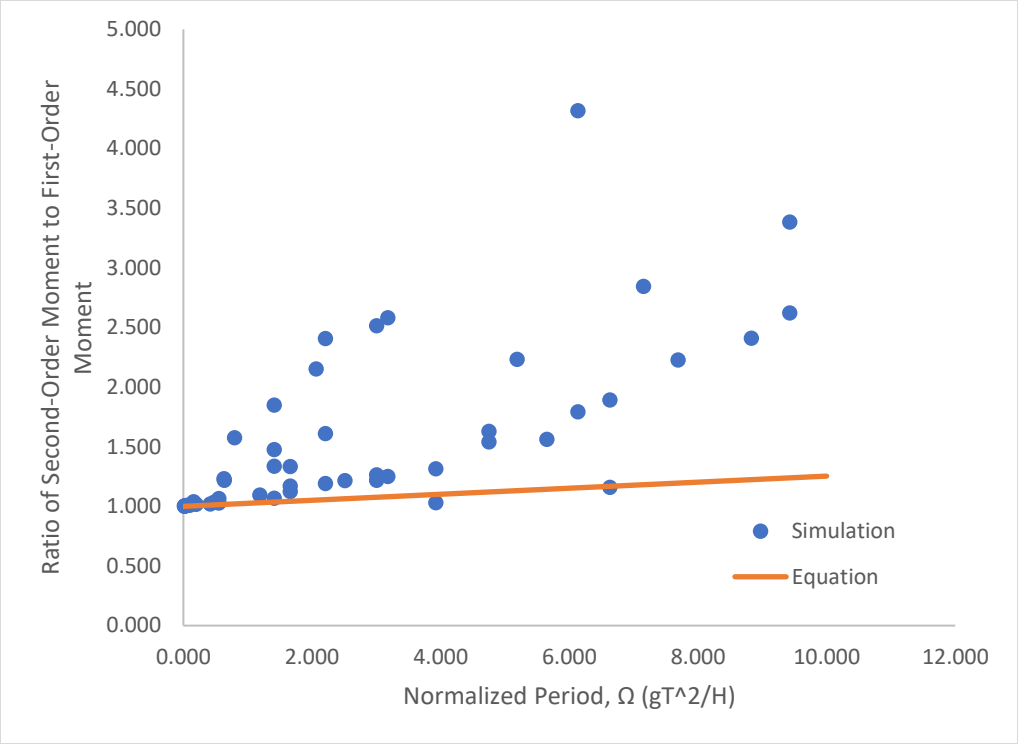

Figure 6: Single Degree of Freedom SAP2000 testing

3.2 Two-Dimensional Verification Structure

To validate required SAP2000 conditions for the second-order and material plasticity analyses, a benchmark OpenSees example is used. The structure, shown in its deformed shape in Figure 7, is a two-story, one-bay structure in two-dimensions and includes a leaning column. The bay width was 360 in, the first-floor height was 180 in, and the second-floor height was 144 in (Eads, 2012). W27x102 and W24x131 sections were used for the beam and column members in the structure, respectively (Eads, 2012). The leaning column, with a rectangular 29x35 inch section, had a much larger area (1000 in^2) and moment of inertia (100,000 in^4) compared to the frame to represent the rest of the structure's affects. The leaning column was connected to the frame through axial members. Plastic hinges were located at 10% of the member length on either end of the member. The hinge length is defined as 0.004 of the length of the associated member (Eads, 2012). The load carrying capacity is extended to generate a longer pushover response. The interaction surface properties are defined from material

properties, and the axial load-displacement relationship was specified as proportional to the moment-based rotation.

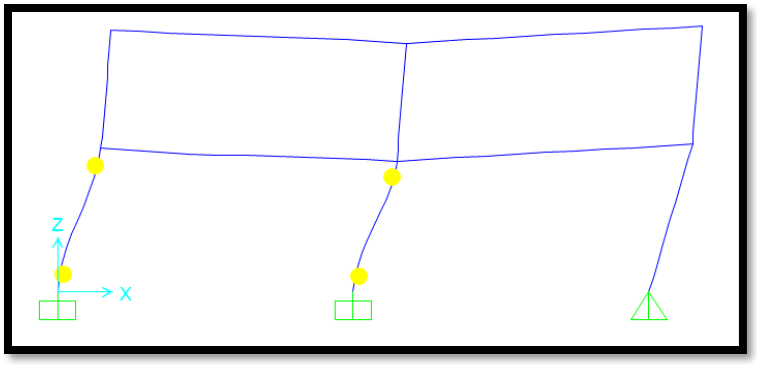

Figure 7: Two-Dimensional Verification Model- Deformed Shape

A static increasing load was applied to the top left corner of the structure to conduct a pushover test. During the test, the column elements began to yield, indicating that they were stiffer than the beam elements. To ensure the hinges were applied correctly, the pushover curve of the modeled structure was compared with the expected pushover curve, both shown Figure 8. The analysis accompanying this example included a normalized comparison between the static pushover curves in OpenSees and SAP2000, so the model could be accurately compared. From the model pushover curve, the response increases nearly linearly until a base shear of about 1880 kip, and remains nearly constant until a tip displacement of 3.9 inches. This shape matches the shape of the published pushover curve. Using the weight and height of the structure, those benchmarks compare to normalized values of 0.27 kip/kip and 0.03 in/in.

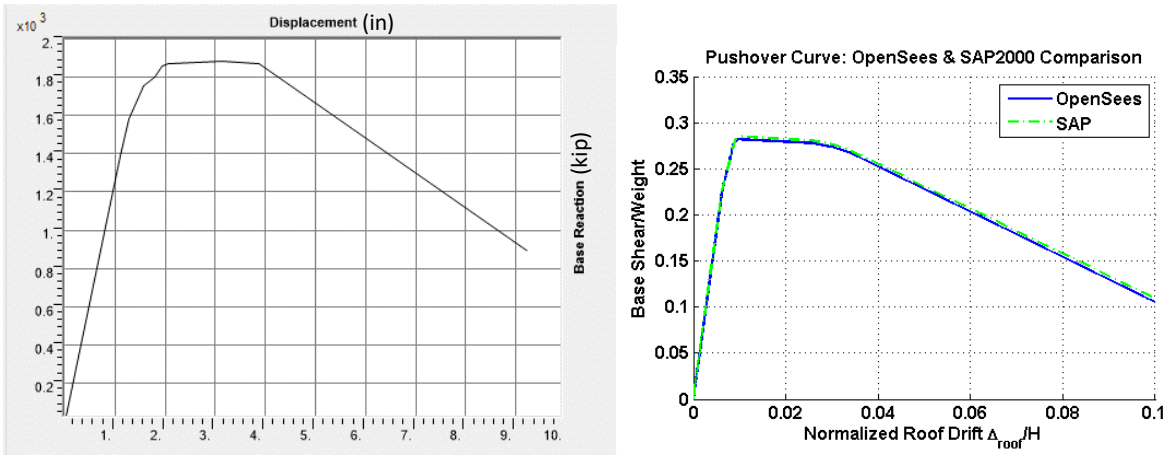

Figure 8: Two-Dimension Pushover Curves: Modeled (left) and Expected (right) (Eads, 2012)

3.3 Three-Dimensional Verification Structure

After confirming hinge parameters using the OpenSees example, a three-dimensional published structure is used to compare the nonlinear tests of a 3-dimension steel moment frame system with concrete floors. Each bay and story height of the six-story structure is set at 4.5 meters (Srinivasu, 2013). As the simulation was conducted by a group of Indian researchers, Indian-standard sections are defined for Fe250 steel. The SAP2000 design feature is used to select appropriate section members for the structure. The chosen frame section assignments are shown in the model in Figure 9. Fe415 steel (modulus of 21 kN/mm^2) and M25 concrete (modulus of 2.5 kN/mm^2) were used in for the 115mm thick floors (Srinivasu, 2013). Hinges are defined as they are in the OpenSees verification structure, and elements were subdivided into three parts to capture the additional, smaller P-delta effect from deflection deviation from the frame's original chord.

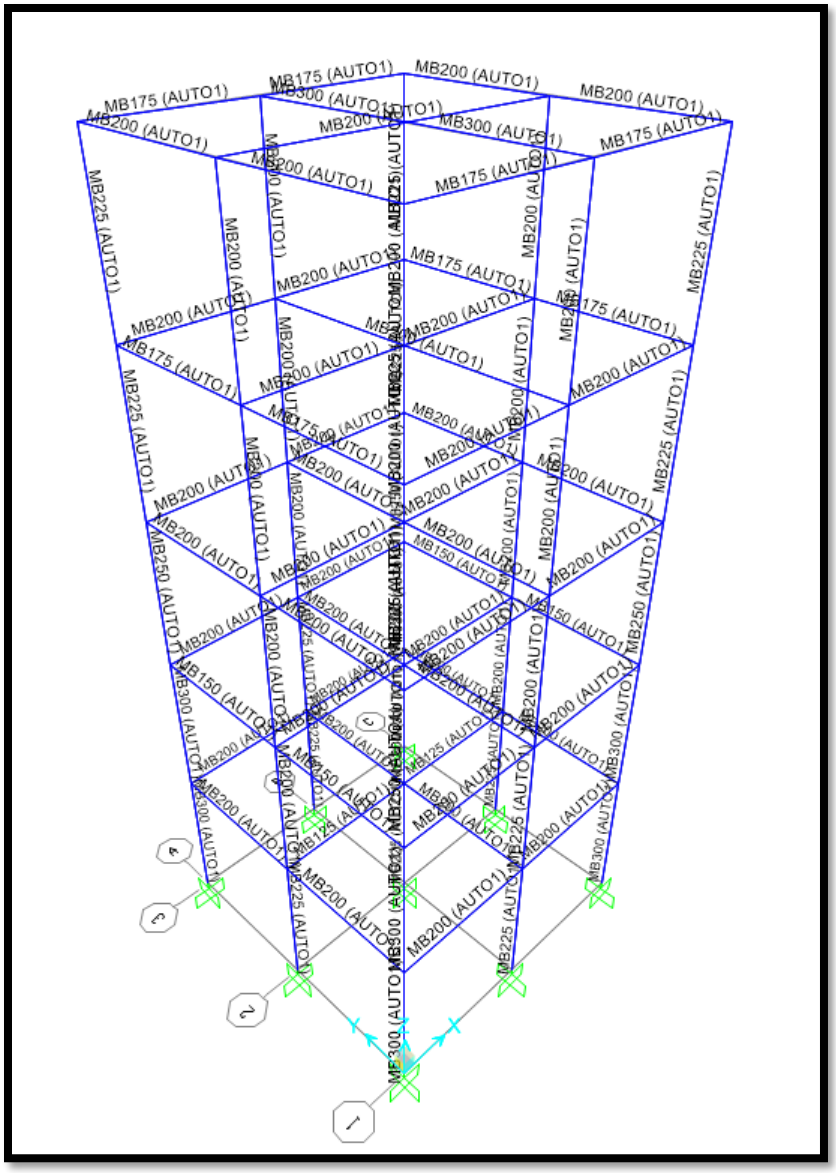

Figure 9: 3D Verification Structure Frame Assignments

A static pushover analysis is conducted for this structure. The hinges activated in the modeled structure match the published structure in location and the approximate amount yielded. The two yielded images are shown in Figure 10, and the two pushover curves are presented in Figure 11. Although the two curves are shown on different x-axis scales, they match well when different points are compared. For example, there is a slight inflection point between linear portions at a displacement value of 2.5m and force of 160 kN on the modeled structure, and corresponding points on the

published structure at about 3m and 200 kN. The linear portion on the modeled structure ends at a displacement of about 4.2m and shear of 280kN, while the end of the linear region on the published structure is at 4.8m and 350kN.

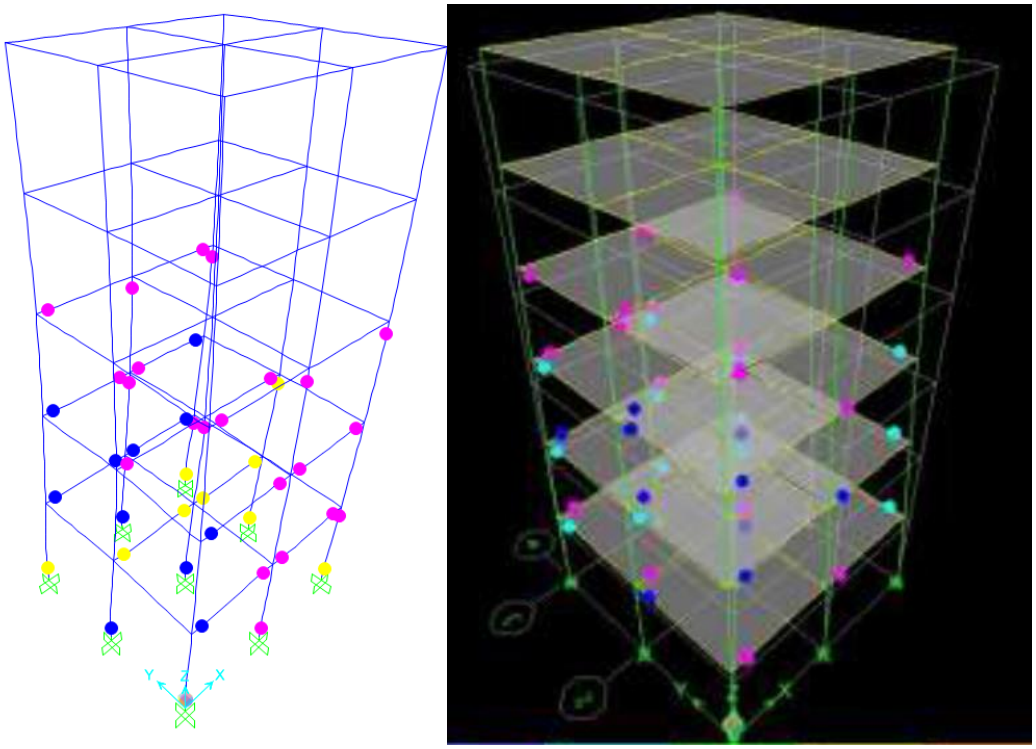

Figure 10: 3D Verification Hinge, Modeled (left) vs Published (right) (Srinivasu, 2013)

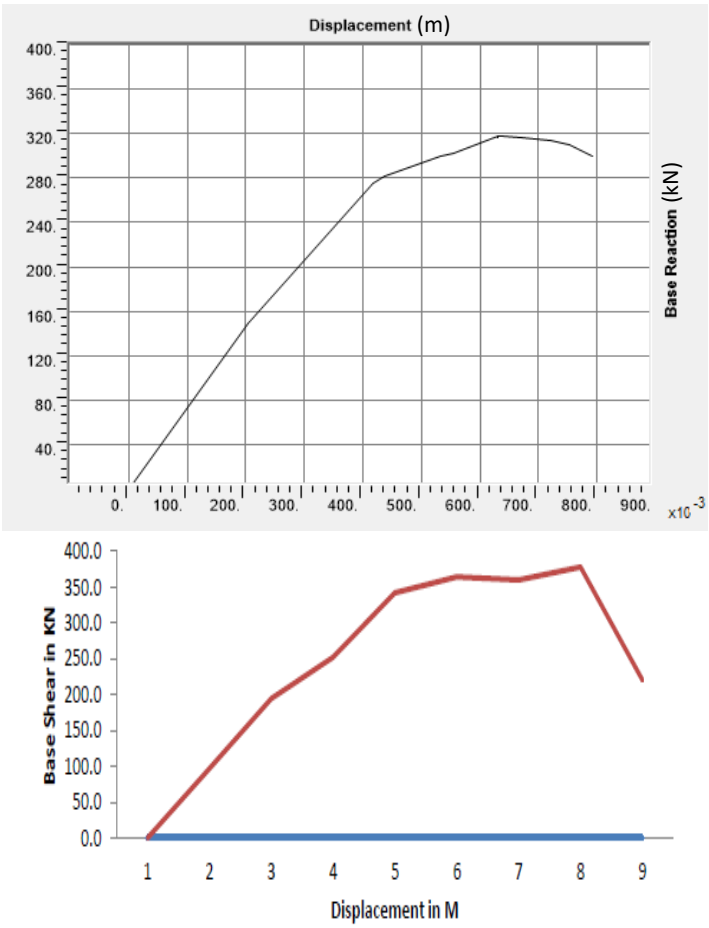

Figure 11: 3D Pushover Curve, Modeled (top), Published (bottom), (Srinivasu, 2013)

CHAPTER 4. HIGH-RISE MODELS

4.1 Ground Motions

For preliminary analyses, the structures were subjected to harmonic excitation, used for a basic time history analysis, with modal damping of 2% and 5%, respectively. A large period of 5 seconds was chosen to mimic naturally occurring long period ground motion. As with all successive analyses, the direct integration method was favored over modal analysis. The Hilber-Hughes-Taylor integration method was used with an alpha parameter of zero, making it equivalent to the Newmark method.

Historical earthquake data with large periods was taken from the PEER database to be used in the analysis. The Kocaeli (1999) and Tohoku (2011) earthquake data was used. Each of these earthquakes registered severe ground shaking and long-period motion. The predominant period of the Kocaeli and Tohuku earthquakes was 1.4 and 3.2 seconds respectively. They had mean periods of 1.3405 and 0.20548 seconds respectively. The acceleration data is presented in Figure 12 and Figure 13.

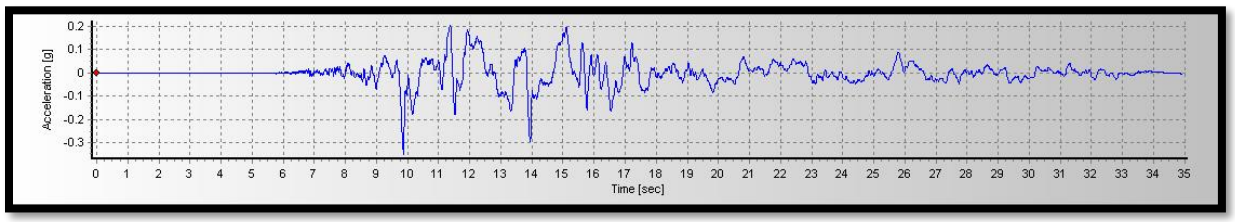

Figure 12: Koceali Ground Acceleration Time History (PEER, 2014)

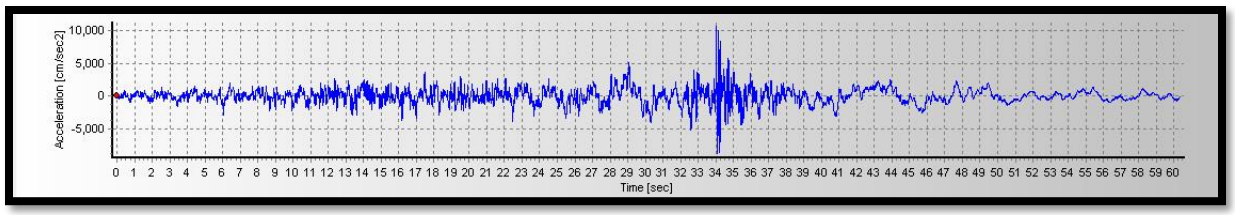

Figure 13: Tohoku Ground Acceleration Time History (PEER, 2014)

The Koceali earthquake occurred on August 17, 1999 and had an intensity of 7.4. It occurred on the North Anatolian fault, and data was recorded at the Yarimca station. This station was only 4km

from the rupture plane and passed through soft soil at the site (Sezen, 2006). The soft soil causes acceleration amplification that can yield a more intense response. Los Angeles, USA and Osaka, Japan also have soft soil basins under developed sites. The Tohoku earthquake acceleration data was recorded at the Osaka station. Although Osaka was over 770km from the epicenter of the 9.1 magnitude earthquake, there was large amplification as predicted by surface-wave amplification theories (Tsai, 2017).

The Tohoku data obtained from the database was in its raw form, so the Seismosignal tools for baseline correction and filtering were used. A linear baseline correction was applied to data for all directions. Butterworth filtering of order 2-4 was also used because of the noisy signal and excessive, unrealistic ground displacements at the end of the series. The Butterworth filtering was selected because it retained most present frequencies, i.e. it was not a low-pass or high-pass filter. The "corner frequencies" in the filtering were selected based on the frequency bounds of the data. The East-West ground motion had the highest acceleration and was used in the analysis.

Simulated ground motion is selected from the Aagaard et al. source model, which provides online time history data. The model with a hypocenter in Bodega Bay was selected with the site label SF472, which corresponds to downtown San Francisco (latitude=37.7750, longitude=-122.4183) (Aagaard et al., 2008). This accelerometer data is presented in Figure 14. Olsen et al. had previously looked at the response of the San Francisco area to the simulated earthquakes with hypocenters near Bodega Bay and San Juan Bautista in Figure 15. Of these, the Bodega Bay had a larger peak ground displacement across the region and in the San Francisco downtown.

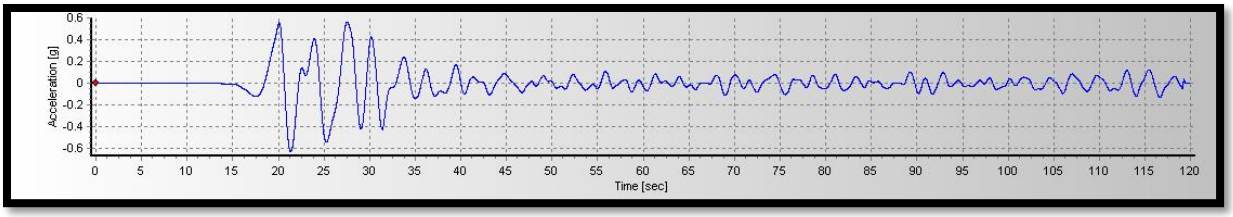

Figure 14: Simulated Ground Motion Time History

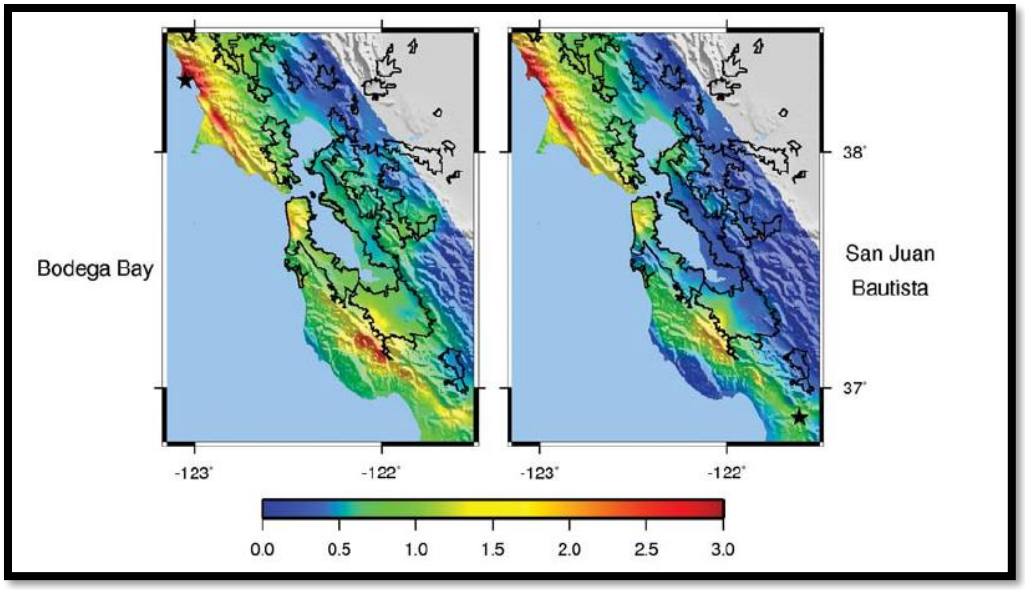

Figure 15: Peak Ground Displacement due to Simulated Earthquakes, in meters (Olsen et al., 2008)

4.2 Nine-Story Benchmark Structure

To best capture an accurate structural response, benchmark and fully-constructed building plans were used. The modeled nine-story structure is part of the SAC project. The nine-story steel structure uses moment resisting frames and pinned ground connections. Lateral pinned connections between the basement and ground floor restrict movement. The frame supports 3-inch thick reinforced concrete floors, and its layout is shown in Figure 16. The overall structure height is 37.19m, while its plan is a 45.73m square. The columns are made of 345MPa steel, and the beams are made of 248MPa steel. The seismic mass of the structure is 9×10^6 kg. Plastic hinges are also applied in the way determined in the verification structures. (Ohtori et al., 2004).

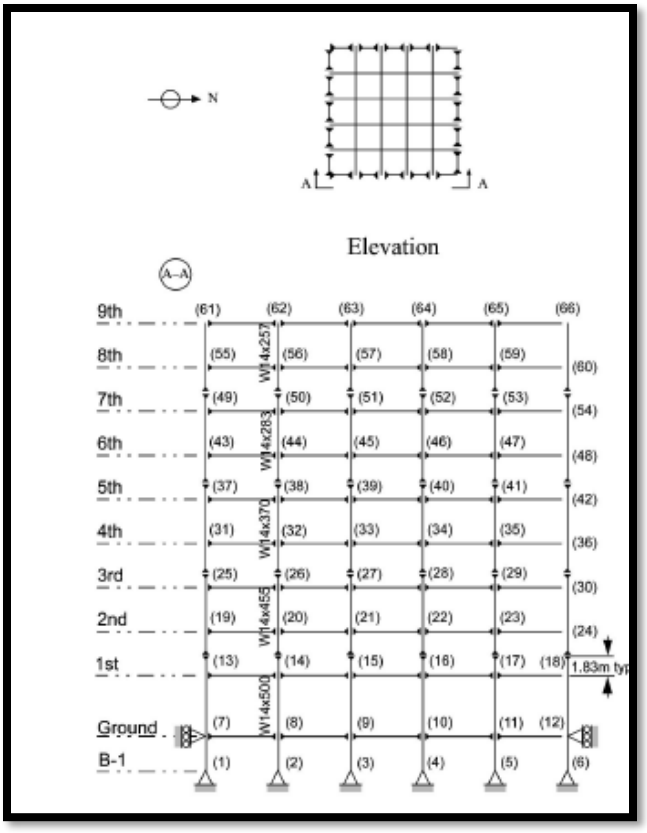

Figure 16: Nine-Story Benchmark Structure (Ohtori et all, 2004)

Before the time history analysis is conducted, the modeled structure's natural frequencies are compared to those listed in Ohtori et al. The first modal frequency listed is 0.44 Hz, while the constructed model had a first modal frequency of 0.41 Hz (Ohtori et al., 2004). The slight discrepancy could be due to the ambiguity of concrete floor thickness in the structure and possible material or shape changes that have occurred in design codes since 2004.

4.3 Twenty-Story Benchmark Structure

The modeled twenty story structure was also developed through the SAC project. This structure has plan dimensions of 30.48m and 36.58m, and a height of 80.77m. The lateral system has exterior moment frames connected by simply supported beams. As in the nine-story structure, the columns are made of 345MPa steel, and the beams are made of 248MPa steel, and the layout is shown in Figure 17. The seismic mass of the structure is 1.11 x 10^7 kg. The first mode had a natural frequency

of 0.19 Hz in the replicated model and 0.26 Hz in the published data. Although the model natural frequency was not replicated exactly, the analysis proceeded with the lower-frequency model because it corresponded with a higher period and was an alternate realistic structure. As it had a higher period, the structural tip displacement would be closer to the maximum ground displacement.

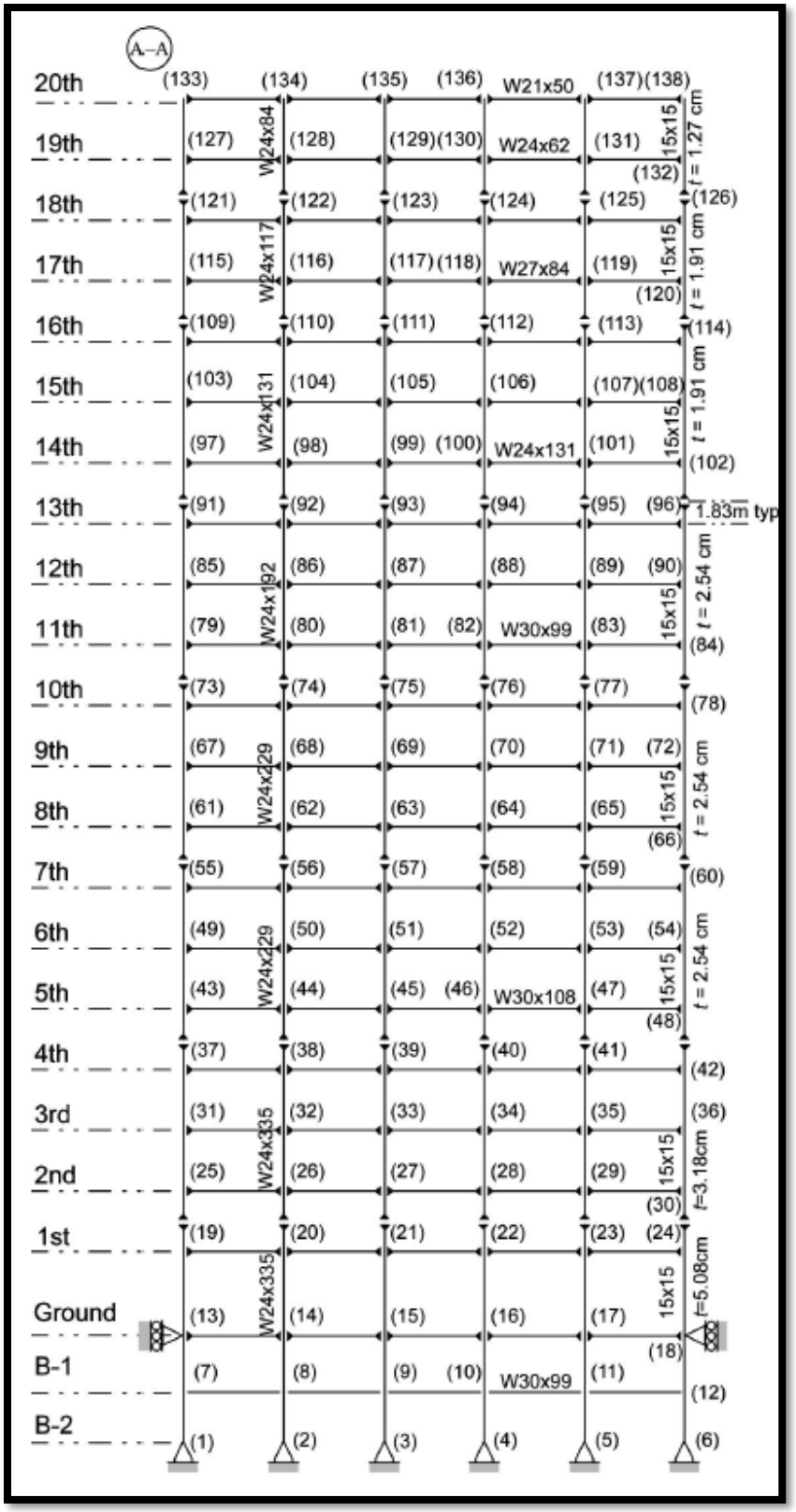

Figure 17: Twenty-Story Benchmark Structure (Ohtori et al., 2004)

CHAPTER 5. RESULTS

5.1 Nine-Story Benchmark Structure

Using the base reaction, the ratio of second-order moment and displacement to their first-order counterparts are calculated and tabulated in Table 1. The ratios for the sine, Tohoku, and simulated ground excitations all appear to have moment amplification ratios of around 5%. This agrees with the moment ratios calculated with Equation 3. These moment ratios are calculated for the first 9 modes of the structure and are presented in Table 2. The equation calculated amplifications have values between 3% and 4%, providing a lower bound for most of the analyzed cases.

Table 1: 9-Story Structure Moment Ratios

Name	Elastic Material Ratio	Inelastic Material Ratio
Sine	1.0454	1.0469
Kocaeli	1.1781	1.0109
Tohoku	1.0713	1.0025
Simulated	1.0454	1.0242

Table 2: 9-Story Structure Modes and Calculated Amplification Factors

Mode	Modal Period (s)	Moment Amplification Factor
1	2.46744	1.037062053
2	2.46513	1.036992691
3	2.46487	1.036984888
4	2.45741	1.036761355
5	2.44009	1.036244988
6	2.52629	1.038851042
7	2.52666	1.038862424
8	2.41193	1.035413241
9	2.4112	1.035391807

The low ratio for some of the inelastic systems could be due to the excessive hinge failure present at the end of the analysis. For example, in the second-order inelastic system analysis of the Tohoku data, nearly all hinges were activated, and many reached the E failure point (Figure 25). Additionally, based on the maximum moments in

Table 3, the Tohoku ground motion caused moments that were much larger compared to the other responses. The 10-17% amplified value of the Kocaeli could be due to partial resonance of one of the higher modes. As the highest modal periods were around 2.4 seconds (Table 2), which is lower than the Tohoku (3.2s), sine (5s), or the simulated (3.48s) predominant periods. This period is larger than the Kocaeli predominant period and, by the nature of listed modal periods, could have another modal period close to 1.4s.

Table 3: Maximum Moments for Ground Excitations and Analyses

	First-Order Elastic Structure (kN-m)	Second-Order Elastic Structure (kN-m)	First-Order Inelastic Structure (kN-m)	Second-Order Inelastic Structure (kN-m)
Sine	698,000	730,000	654,000	684,000
Kocaeli	169,000	199,000	180,000	182,000
Tohoku	1,932,000	2,070,000	1,746,000	1,750,000
Simulated	70,990	74,216	55,288	56,624

There was little amplification for the displacements for all the ground excitations, shown in Table 4. With some variation, there was only a 4% amplification for the top joints of the structure. There were some values that were less than one, indicating that the first-order displacement exceeded the second-order displacement slightly. Most of these occurred in the nonlinear structure, which could be due to the energy released during hinge yielding. The additional energy from the second order analysis could have caused more hinges to develop and rotate, allowing more vertical motion within the member and reducing horizontal motion. For example, the Tohoku nonlinear system had many of the hinges yield, allowing this rotation to proceed; it also had the lowest displacement amplification of 0.77 at one of the top corner joints.

Table 4: 9-Story Structure Displacement Ratios for Tip Joints (L is for the linear structure and N is for the Nonlinear Structure)

	Joint 1		Joint 2		Joint 3		Joint 4		Joint 5		Joint 6	
	L	N	L	N	L	N	L	N	L	N	L	N
Sine	1.03	1.01	1.04	1.03	1.04	1.03	1.04	1.04	1.04	1.04	1.03	1.02
Koc.	1.02	1.02	1.01	1.01	1.01	1.01	0.99	0.99	0.99	0.99	1.02	1.02
Toh.	1.02	0.77	1.04	1.06	1.04	1.07	1.04	0.90	1.04	0.90	1.02	0.77
Sim.	1.03	1.03	1.04	1.03	1.04	1.03	1.04	1.03	-	1.03	-	1.03

The maximum tip joint displacements, in Table 5, reflected the same trends present with the maximum moment data. The Tohoku excitation caused the largest displacements, an order of magnitude larger than the other displacements. Additionally, the displacements did not vary based on whether they were interior or exterior joints, but the interior joints deformed more.

Table 5: Maximum Displacement at 2 Joints (Exterior and Interior)

	1st Joint (m)				2nd Joint (m)			
	1st Linear	2nd Linear	1st Non.	2nd Non.	1st Linear	2nd Linear	1st Non.	2nd Non.
Sine	0.814	0.846	0.800	0.823	0.852	0.883	0.852	0.883
Koc.	0.185	0.186	0.185	0.186	0.203	0.201	0.203	0.201
Toh.	3.170	3.289	2.438	2.600	3.365	3.514	2.913	2.633
Sim.	0.070	0.072	0.070	0.072	0.090	0.093	0.090	0.093

5.1.1. Sine Excitation:

The difference in first-order and second-order effects in the deformed shapes are more prominent when looking at the nonlinear structure because of change in hinge use. The hinges utilized in the first-order analysis yield more in the second-order strucure, particularly on the roof and 6th floor of the structure, as shown in Figure 18.

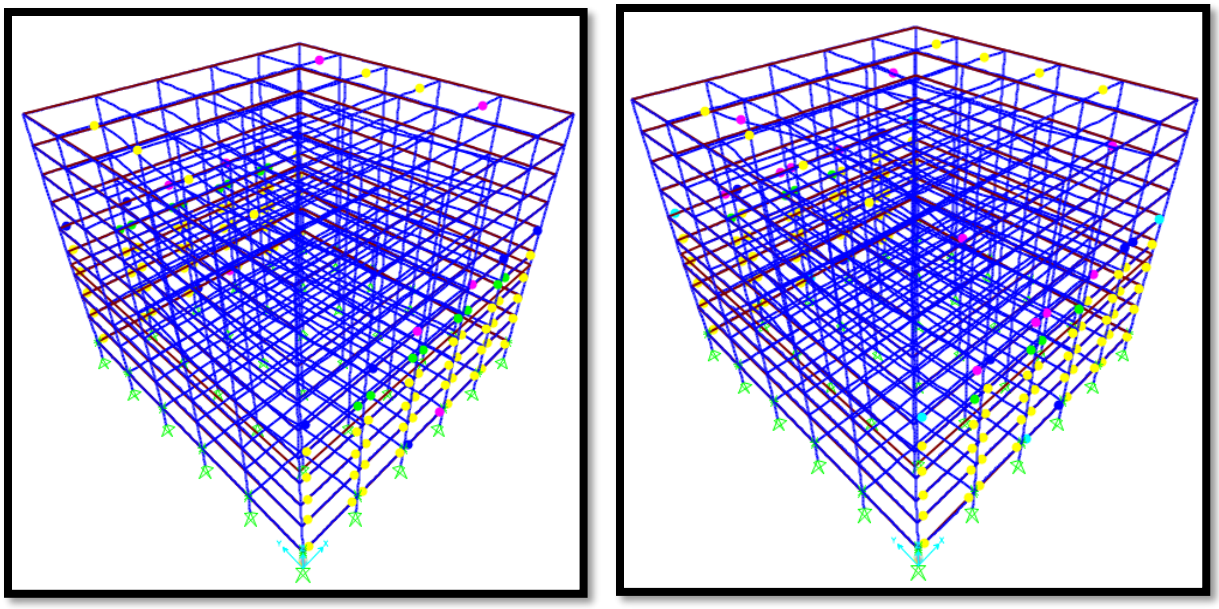

Figure 18: Deformed 9-Story Nonlinear Structure, Sinusoidal Excitation: First-Order Analysis (left), Second-Order Analysis (right)

The time history moments are presented in Figure 19, where there moment amplification is more noticeable when there is a positive moment. Additionally, the peak second-order moments seem to be shifted slightly from the first-order moments. This is possibly due to how the initial weight effects are considered in the SAP2000 second-order analysis. The second-order analysis begins at a reduced stiffness in accordance with after the dead weight is applied.

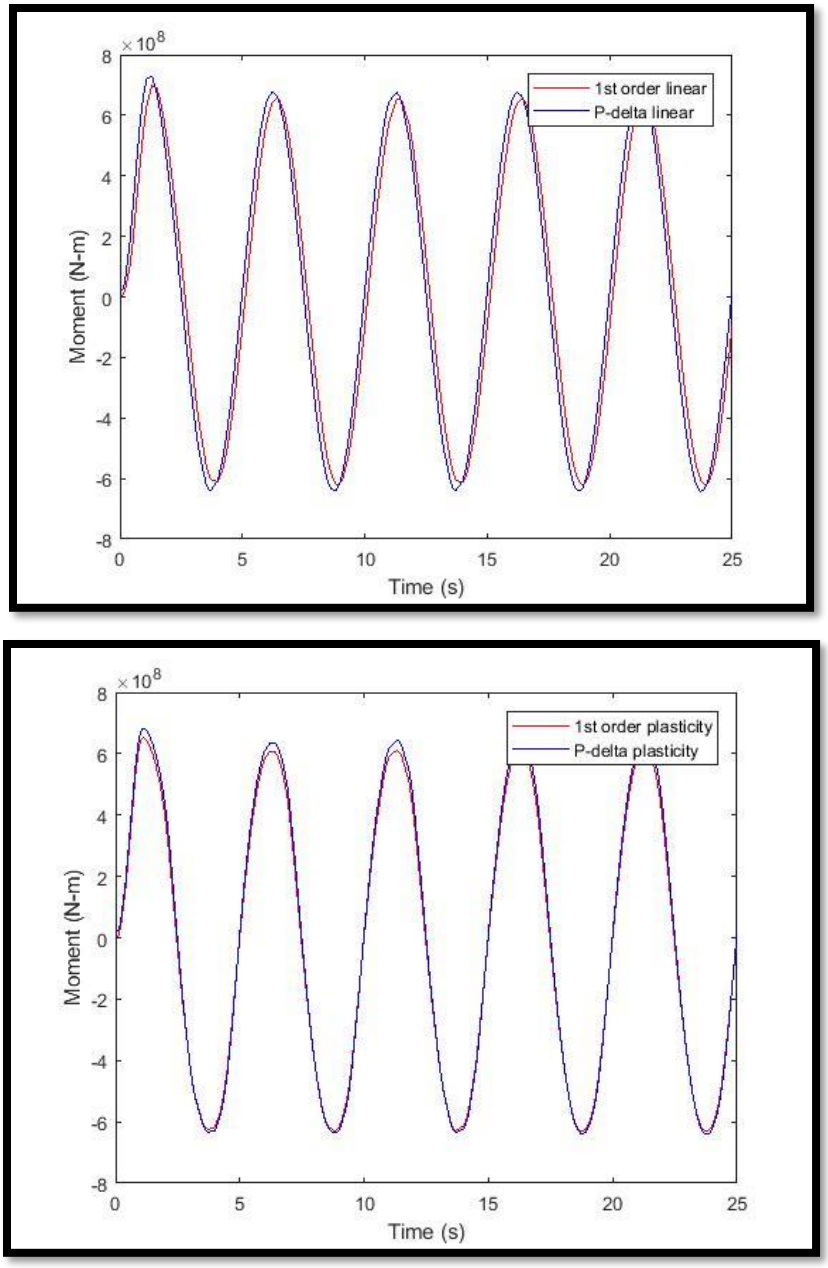

Figure 19: Moment Response Time History, Sinusoidal Motion:9-Story Linear Structure (Top), Nonlinear Structure (Bottom)

The time history tip displacement for the linear and nonlinear structures are shown in Figure 20 and Figure 21. Because of the lower amplification ratios and scale of the image, it is more difficult to differentiate the first-order analysis from the second-order analysis. As in the moment time history, the displacement repeats throughout the analyzed time because of the repeating sinusoidal excitation.

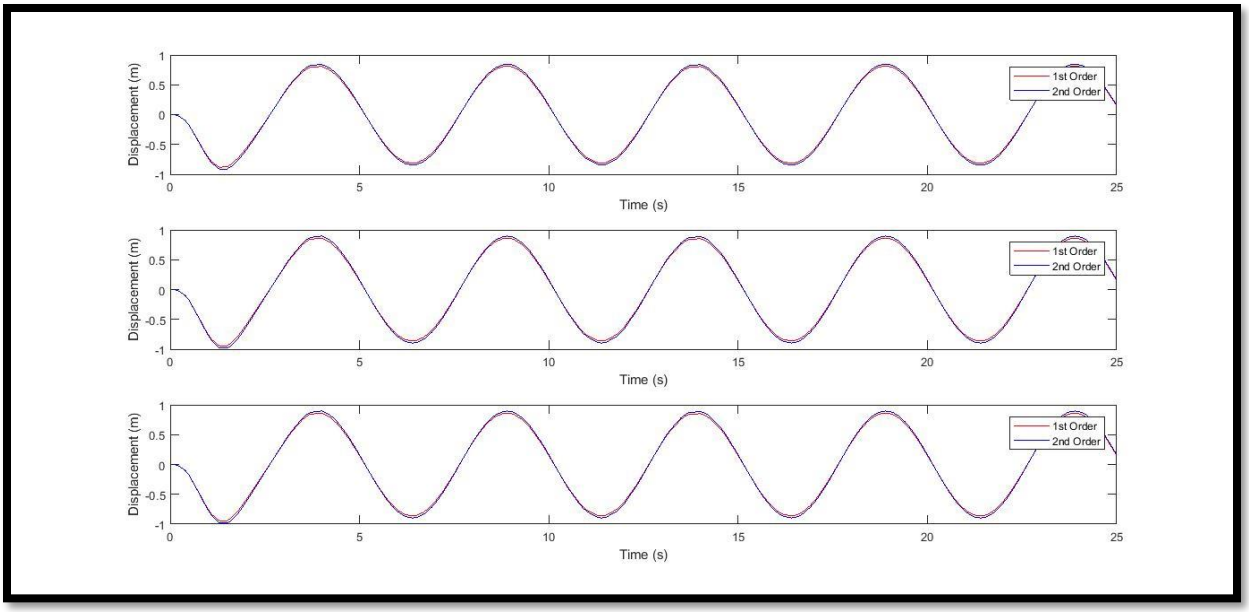

Figure 20: Tip Joint Displacements for 9-Story Linear Structure, Sinusoidal Motion

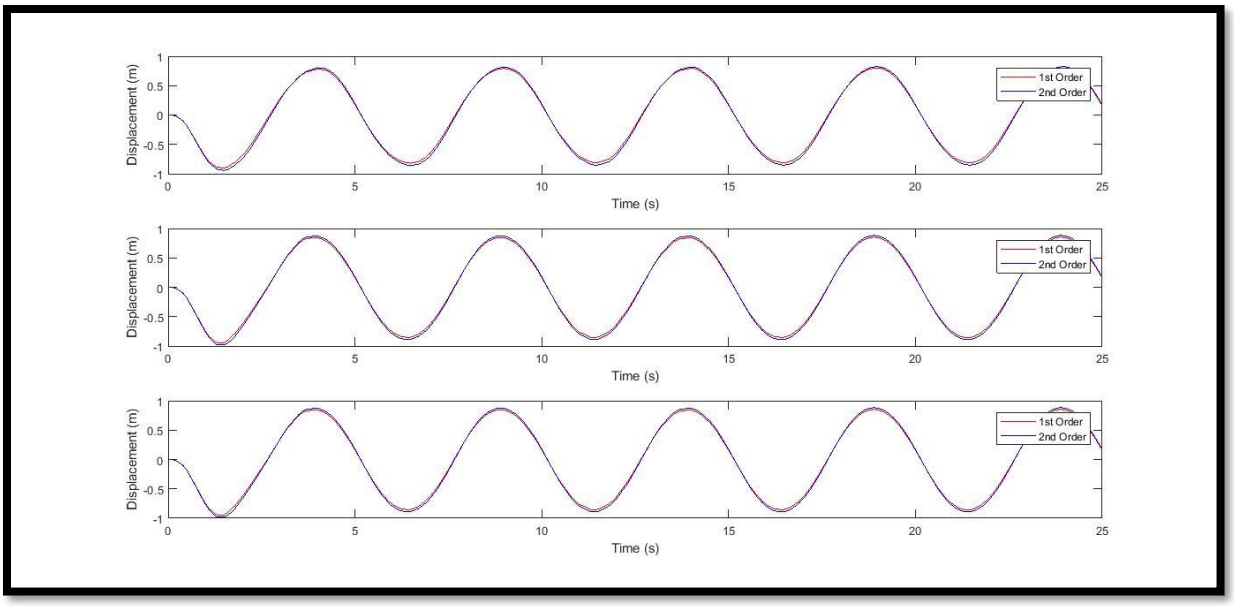

Figure 21: Tip Joint Displacements for 9-Story Nonlinear Structure, Sinusoidal Motion

5.1.2. Kocaeli Ground Motion:

The moment response time history, presented in Figure 22, follows the ground motion excitation. As demonstrated by the calculations in Table 1, the amplification is more pronounced in the linear material model. Both moments follow the ground exciatation in the linear and nonlinear

material models, but the differences are most prominent at the local maxima and minimums. It is the only location where the difference can be seen in the nonlinear material plot.

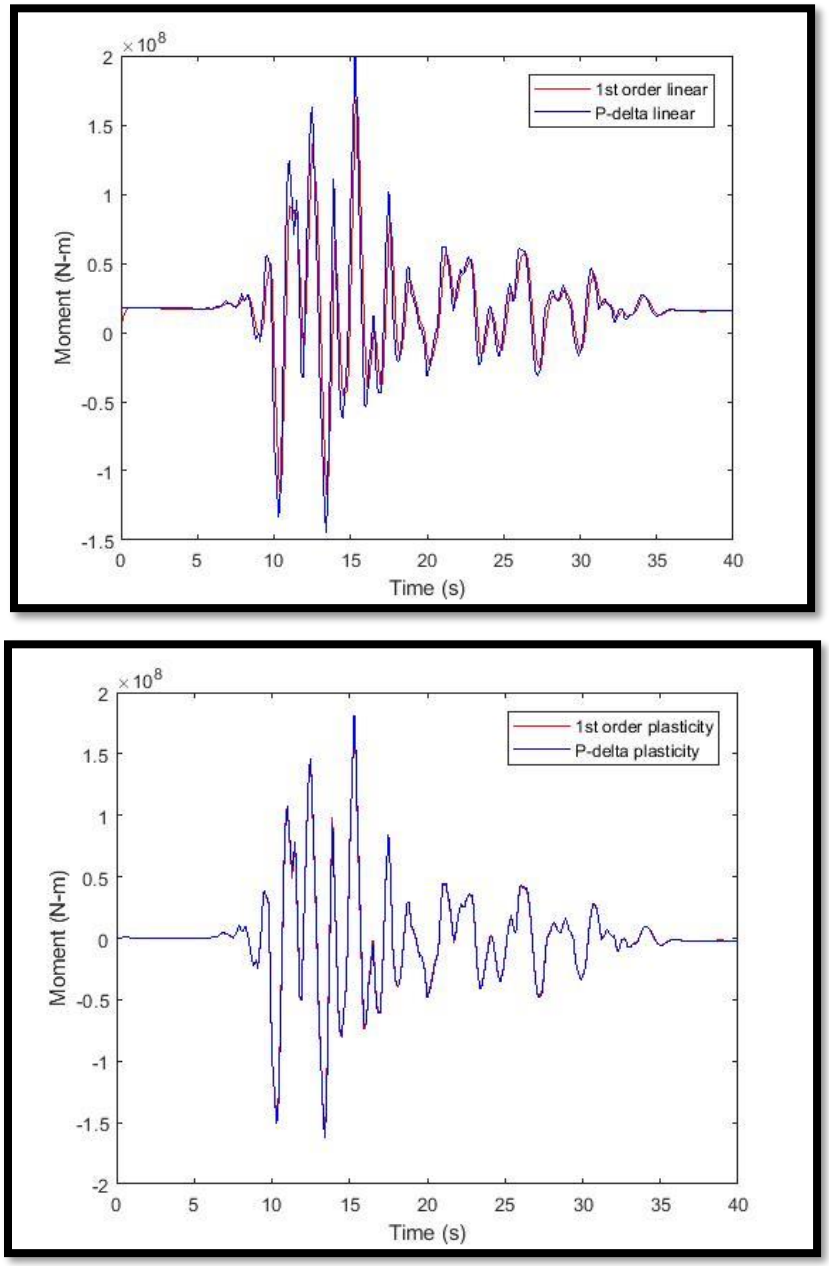

Figure 22: Moment Response Time History, Kocaeli Motion: 9-Story Linear Structure (Top), Nonlinear Structure (Bottom)

The displacement time history for the linear and nonlinear structure follow similar patterns in terms of the time and joint differences. The displacements in Figure 23 and Figure 24 for a set of the

tip joints are similar because of the low amplification ratios. The displacements begin to have peaks where the excitation increases significantly, but the displacement time history does not resemble the ground excitation as it did with the sinusoidal wave.

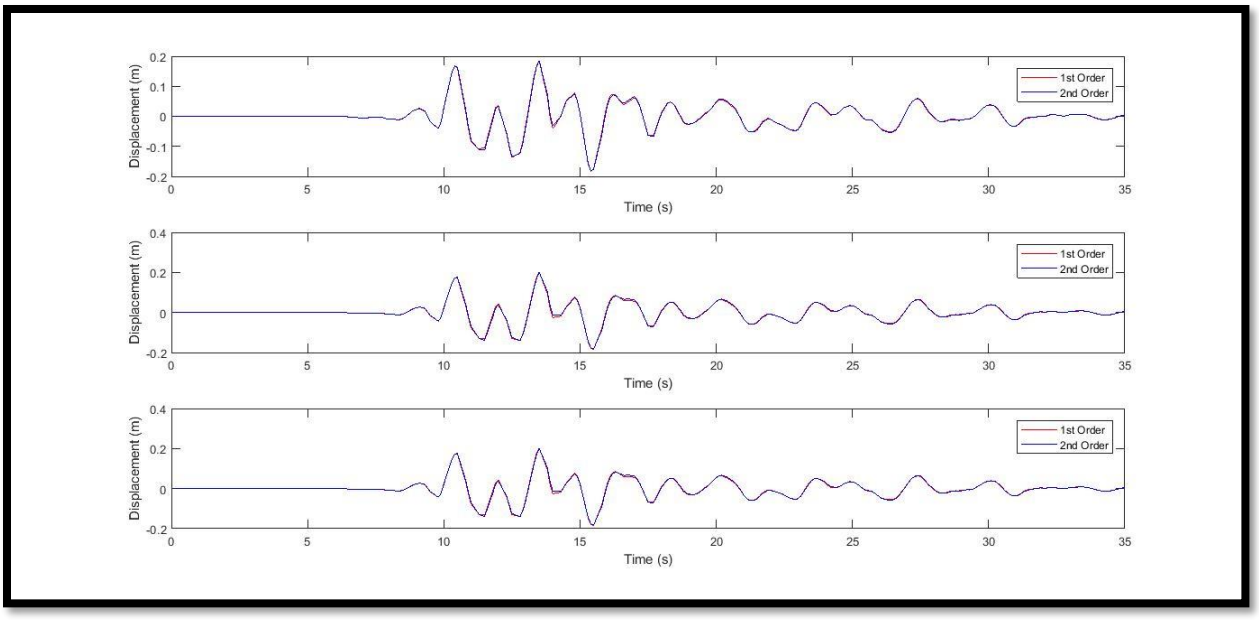

Figure 23: Tip Joint Displacements for 9-Story Linear Structure, Kocaeli Motion

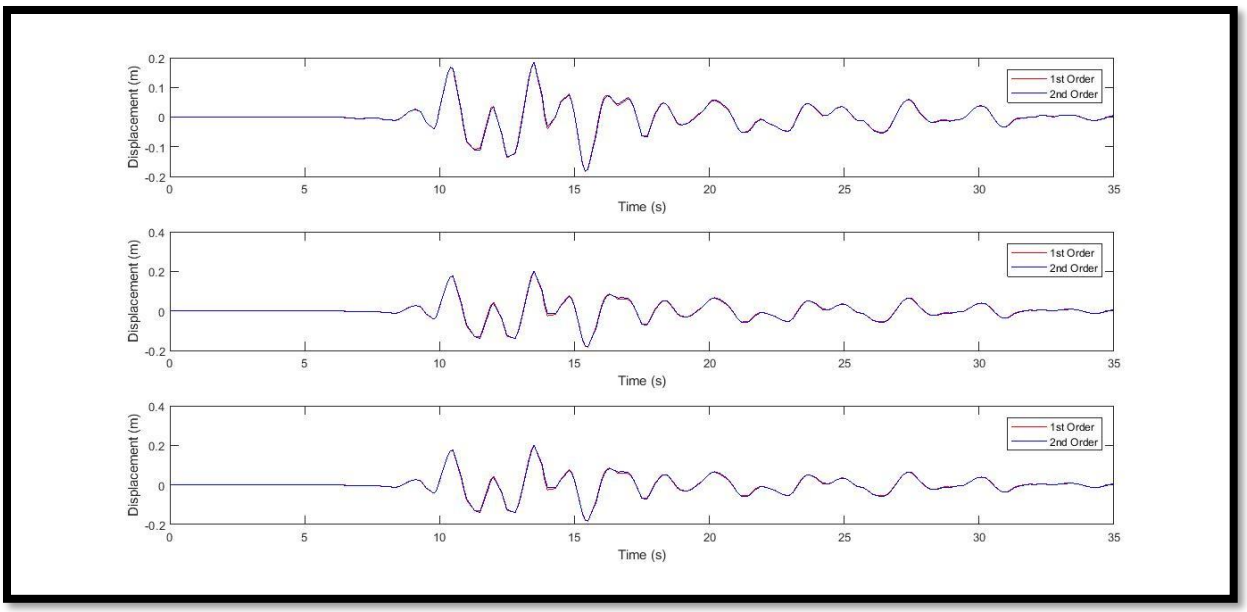

Figure 24: Tip Joint Displacements for 9-StoryNonlinear Structure, Kocaeli Motion

5.1.3. Tohoku Ground Motion:

The Tohoku ground motion had the most intense response of all of the analyzed accelerations. In Figure 25, both the first-order and second analyses yielded significant plastic behavior in the nonlinear structure. Additionally, several more hinges reached their failure point in the second-order analysis compared to the one or two hinge failures in the first-order analysis.

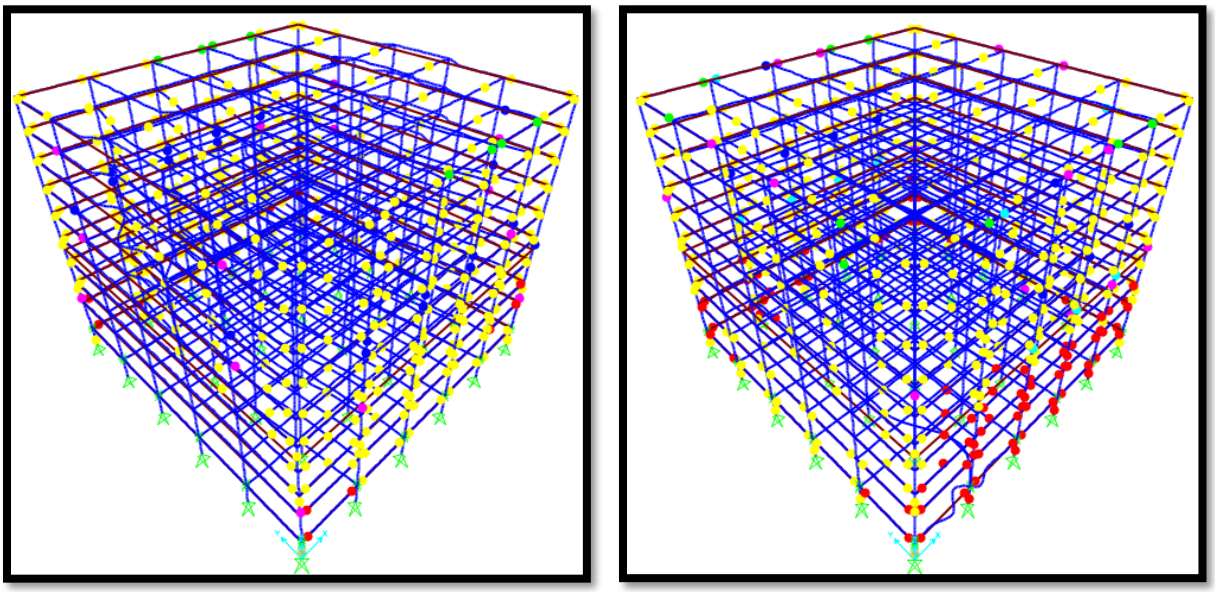

Figure 25: Deformed 9-Story Nonlinear Structure, Tohoku Excitation: First-Order Analysis (left), Second-Order Analysis (right)

The moment response time history for the first-order and second-order analyses follow each other closely. In both the linear and nonlinear structures shown in Figure 26, the second-order moment response was not able to be calculated for the second half of the analysis. This could be due to the structure failing at this point. This seems reasonable due to the large amount of hinge failures in the second-order analysis of the nonlinear structure.

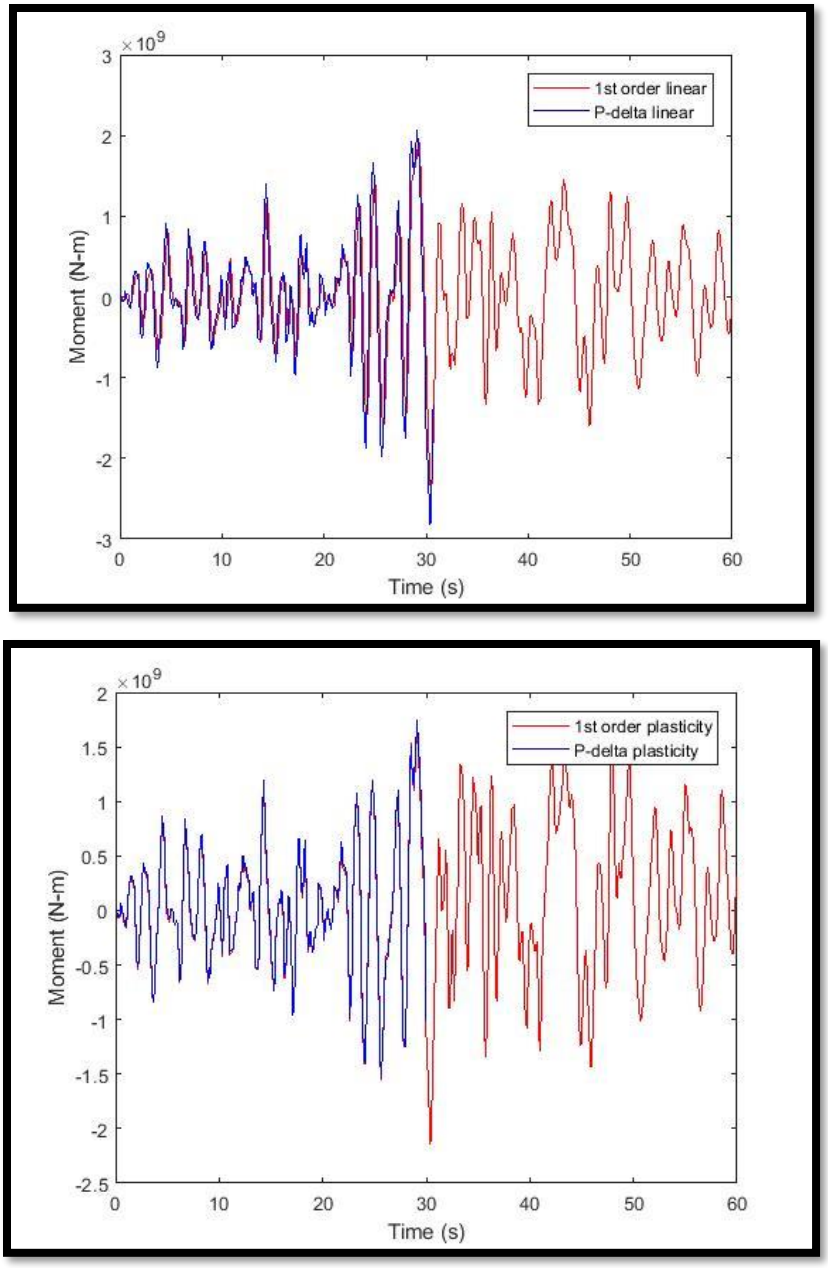

Figure 26: Moment Response Time History, Tohoku Motion: 9-Story Linear Structure (Top), Nonlinear Structure (Bottom)

The response of the displacement time history does not seem to directly follow the ground excitation but have similar patterns to the other displacement time histories. In the linear structure, the displacements in Figure 27 for the first-order and second-order analyses follow each other closely. The nonlinear structure in Figure 28 has the second-order displacement offset from the first-order displacements. This could be due to the moment releases associated with the hinge activation and

yielding. As with the moment time histories, the second-order analyses do not continue past the 30-second time for a long time.

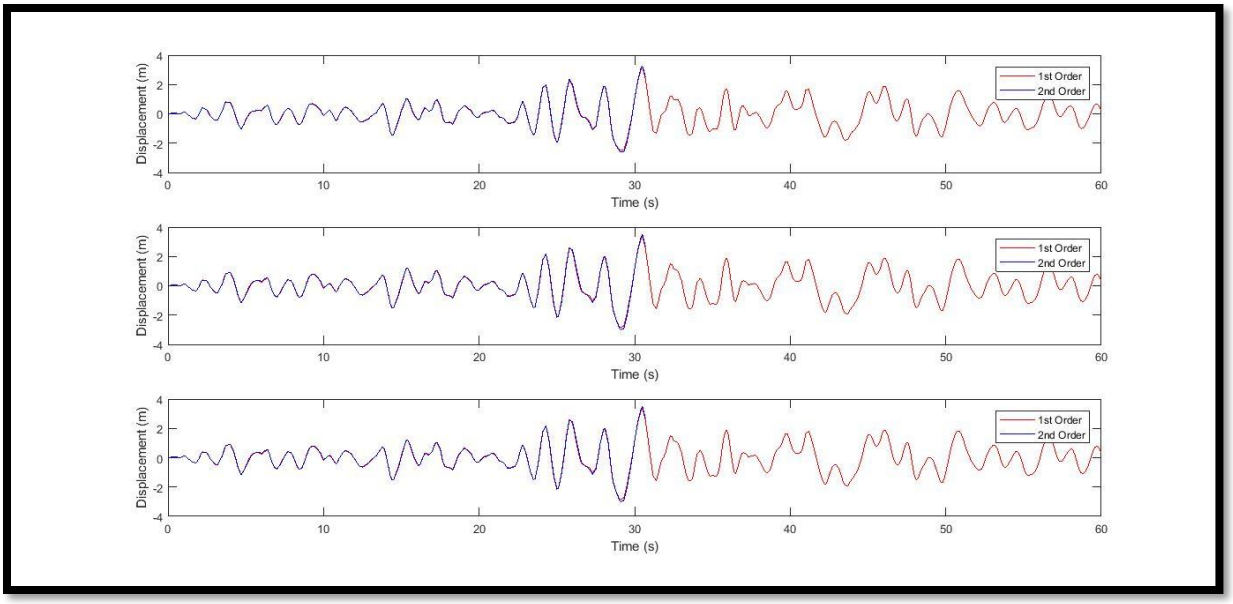

Figure 27: Tip Joint Displacements for 9-Story Linear Structure, Tohoku Motion

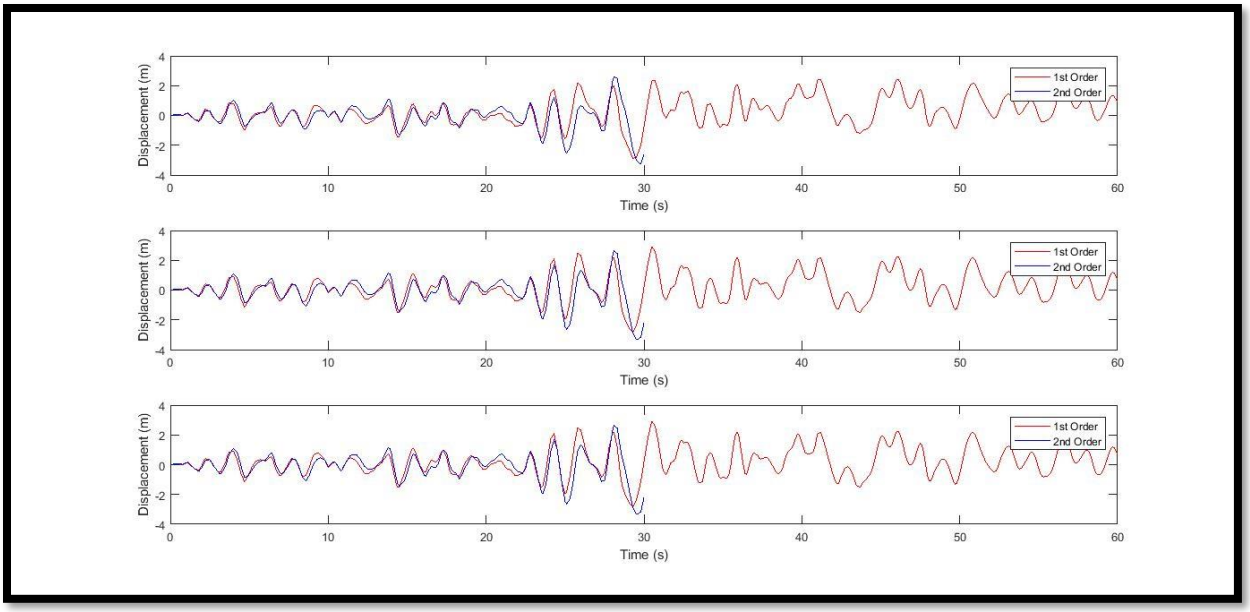

Figure 28: Tip Joint Displacements for 9-Story Nonlinear Structure, Tohoku Motion

5.1.4. Simulated Ground Motion:

The moment time histories follow the ground acceleration, similar to the other moment data. The linear and nonlinear structures in Figure 29 has second-order data that closes follows the first-

order data. As with the Kocaeli ground motion, the difference between the first-order and second-order analyses are more pronounced in the linear structure compared to the nonlinear structure.

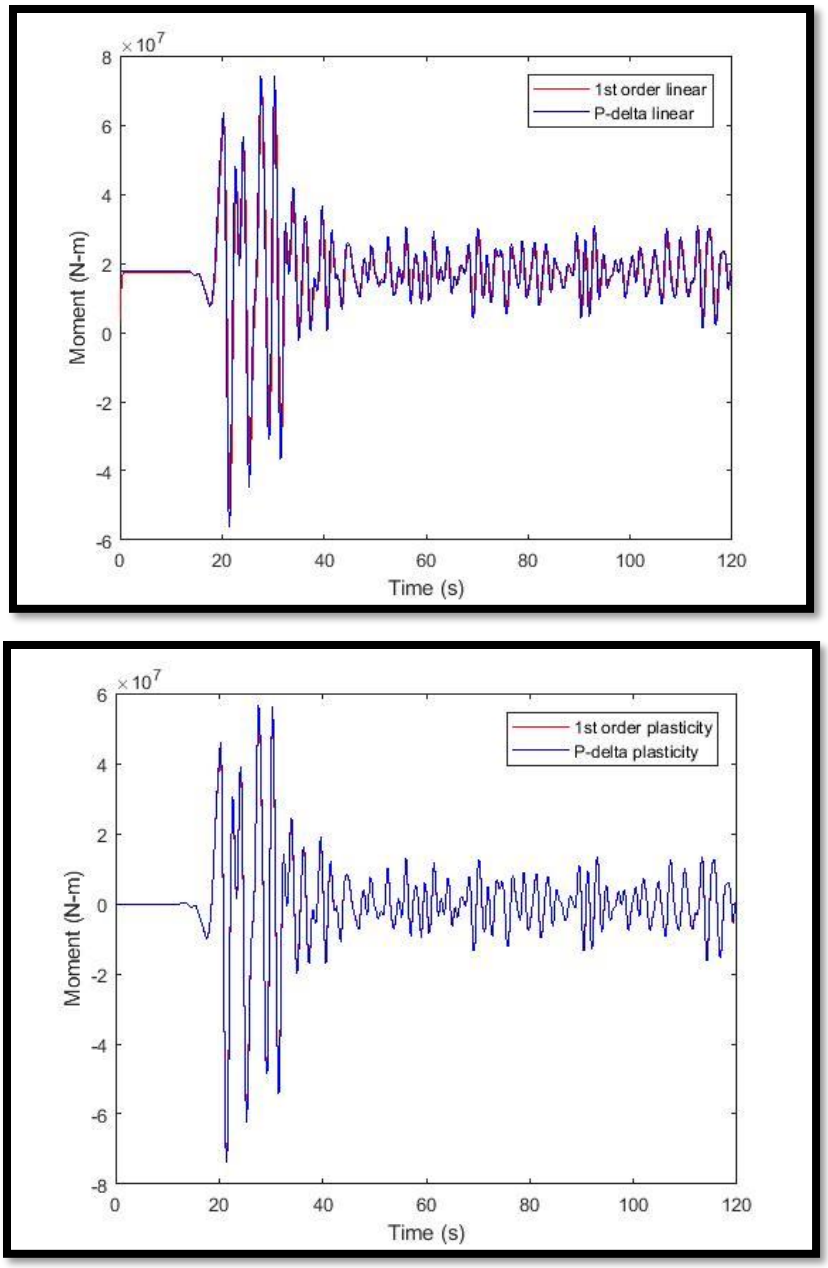

Figure 29: Moment Response Time History, Simulated Motion: 9-Story Linear Structure (Top), Nonlinear Structure (Bottom)

The location of peaks in Figure 30 and Figure 31 follow the ground motion and moment time histories. As there was low amplification due to the simulated ground motion, it is difficult to see the specific differences between the first-order and second-order analyses in the time histories.

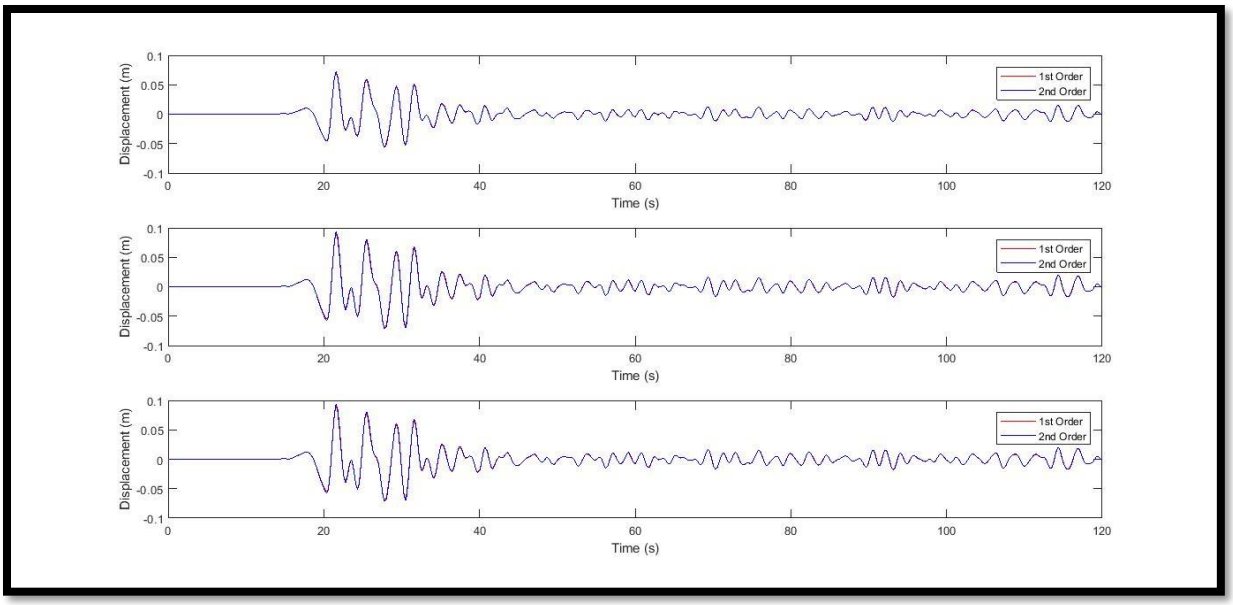

Figure 30: Tip Joint Displacements for 9-Story Linear Structure, Simulated Motion

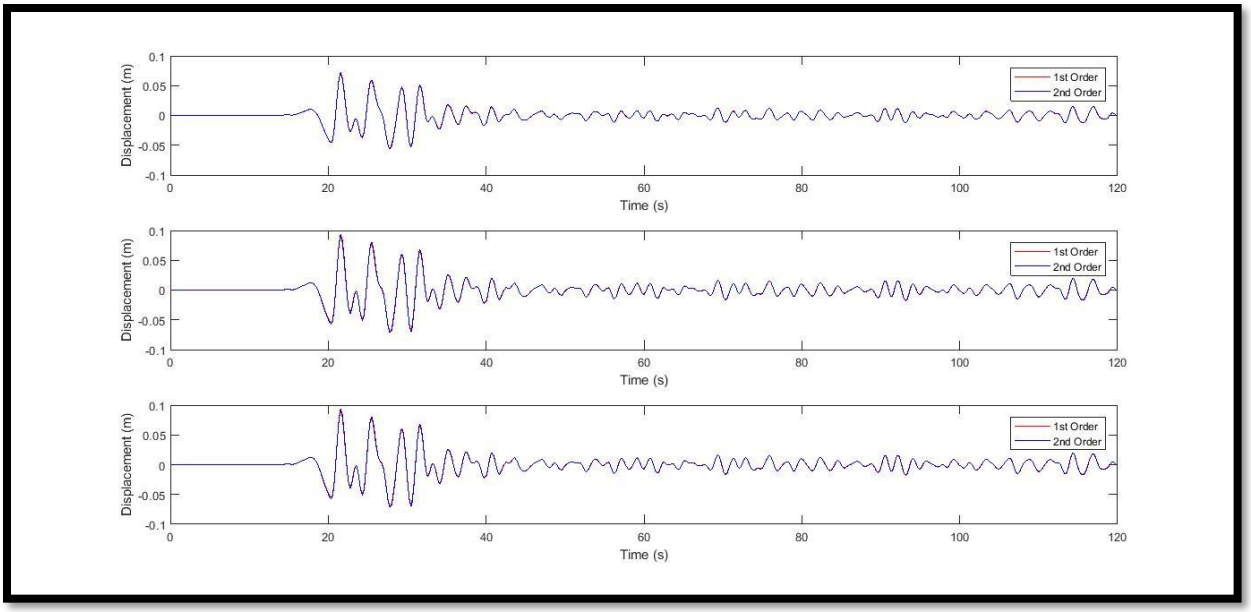

Figure 31: Tip Joint Displacements for 9-Story Nonlinear Structure, Simulated Motion

5.2 Twenty-Story Benchmark Structure

The moment ratios for the 20-story structure varied between a 6% and 10% amplification between the first-order and second-order analysis (Table 6). The predicted amplification values based on mode shapes in Table *7* are more similar to the model results in Table 6 at the higher modal periods. The first mode has an amplification of 7.5%, like the elastic Tohoku amplification. These also provide a lower bound for the Kocaeli amplifications. The lower modal periods agree more with the Sinusoidal and Simulated ground motion amplifications.

Table 6: 20-Story Structure Moment Ratios

Name	Elastic Material Ratio	Inelastic Material Ratio
Sine	1.0536	0.9753
Kocaeli	1.0913	1.0913
Tohoku	1.0794	0.9748
Simulated	1.0646	1.0646

Table 7: 20-Story Structure Modes and Calculated Amplification Factors

Mode	Modal Period	Amplification Factor
1	5.16941	1.075432852
2	3.48965	1.034374969
3	2.27351	1.014590572
4	1.85282	1.009690474
5	1.2338	1.004297027
6	1.15481	1.003764434
7	0.93822	1.00248478
8	0.92319	1.002405807
9	0.82947	1.001942137

For some of the inelastic structures, particularly when subjected to the sinusoidal and Tohoku excitation, there was a slight reduction in the moment when changing from the first-order to second-

order analysis. This could possibly be due to increased yielding and a resultant decreased lateral deformation at some time steps. The deformed inelastic structure showed several failed members in Figure 32 for the sinusoidal excitation and Figure 39 for the Tohoku excitation. Additionally, the maximum moments for these two excitations, listed in Table 8, are almost an order of magnitude larger than the moments for the Kocaeli and Simulated ground motions.

Table 8: Maximum Moment in 20-Story Structure

	First-Order Elastic Structure (kN-m)	Second-Order Elastic Structure (kN-m)	First-Order Inelastic Structure (kN-m)	Second-Order Inelastic Structure (kN-m)
Sine	3,610,000	3,800,000	3,606,000	3,517,000
Kocaeli	793,000	866,000	793,000	866,000
Tohoku	3,849,000	4,155,000	3,849,000	3,752,000
Simulated	640,000	682,000	640,000	682,000

The tip displacements amplifications are lower than the moment displacements for the 20-story building, as it is for the 9-story structure. Compared to the 9-story structure, the 20-story tip displacement amplifications are larger, as they were with the moment amplifications. The amplification values in Table 9 are typically under 10%. Like the 9-story structure, some values are below 1, indicating the first-order displacement was larger than the second-order displacement. Again, most of these values are for the nonlinear structure, where yielding could have reduced the horizontal displacement.

Table 9: 20-Story Structure Displacement Ratios for Tip Joints (L is for the linear structure and P is for the Nonlinear Structure)

	Joint 1		Joint 2		Joint 3		Joint 4		Joint 5		Joint 6	
	L	N	L	N	L	N	L	N	L	N	L	N
Sine	1.04	1.06	1.04	1.07	1.04	1.08	-	1.08	1.03	1.07	1.03	1.05
Koc	1.03	1.03	1.03	1.03	1.03	1.03	1.03	1.03	1.03	1.03	1.03	1.03
Toh	0.99	0.89	1.00	0.89	1.00	0.89	1.00	0.88	1.00	0.89	1.00	0.90
Sim	1.02	1.02	1.02	1.02	1.03	1.03	1.03	1.03	1.03	1.03	-	-

The maximum displacements for the 20-story structure, in Table 10, are also larger than the 9-story structure. The displacement of different joints varied more compared to the 9-story structure. The exterior joint typically had the largest displacement of the locations for the different structures and analyses. As with the maximum moment, there was a much larger displacement due to the Tohoku and Sinusoidal excitations compared to the Kocaeli and Tohoku data.

Table 10: Maximum Interior and Exterior Tip Displacements, 20-Story Structure

	1st Joint (m)				2nd Joint (m)			
	1st Linear	2nd Linear	1st Non.	2nd Non.	1st Linear	2nd Linear	1st Non.	2nd Non.
Sine	1.799	1.863	1.800	1.904	1.355	1.405	1.355	1.454
Koc.	0.278	0.285	0.278	0.285	0.198	0.204	0.198	0.204
Toh.	2.540	2.520	2.540	2.268	1.763	1.755	1.763	1.566
Sim.	0.226	0.231	0.226	0.231	0.167	0.171	0.167	0.171

5.2.1. Sine Excitation:

In the nonlinear structure, shown in Figure 32, shows a large difference between the first-order and second-order yielding. There is very little yielding in the first-order analysis, but many members yielding during the second-order analysis. Several members near the base reached their plastic capacity and yielded as well.

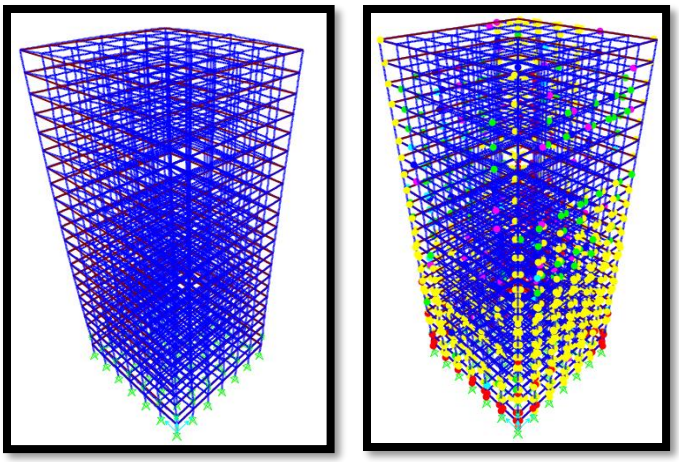

Figure 32: Deformed 20-Story Nonlinear Structure, Sinusoidal Excitation: First-Order Analysis (left), Second-Order Analysis (right)

The moment time history in the 20-story structure follows the same trends as the moment time history for the 9-story structure. A difference is that in the linear structure in Figure 33 has higher first-order and second-order moments at their first peak, and there is a larger amplification. The nonlinear structure's second-order moment is not recorded after about 15 seconds, likely due to the structure's collapse at that time. Given the number of hinge failures, this is reasonable.

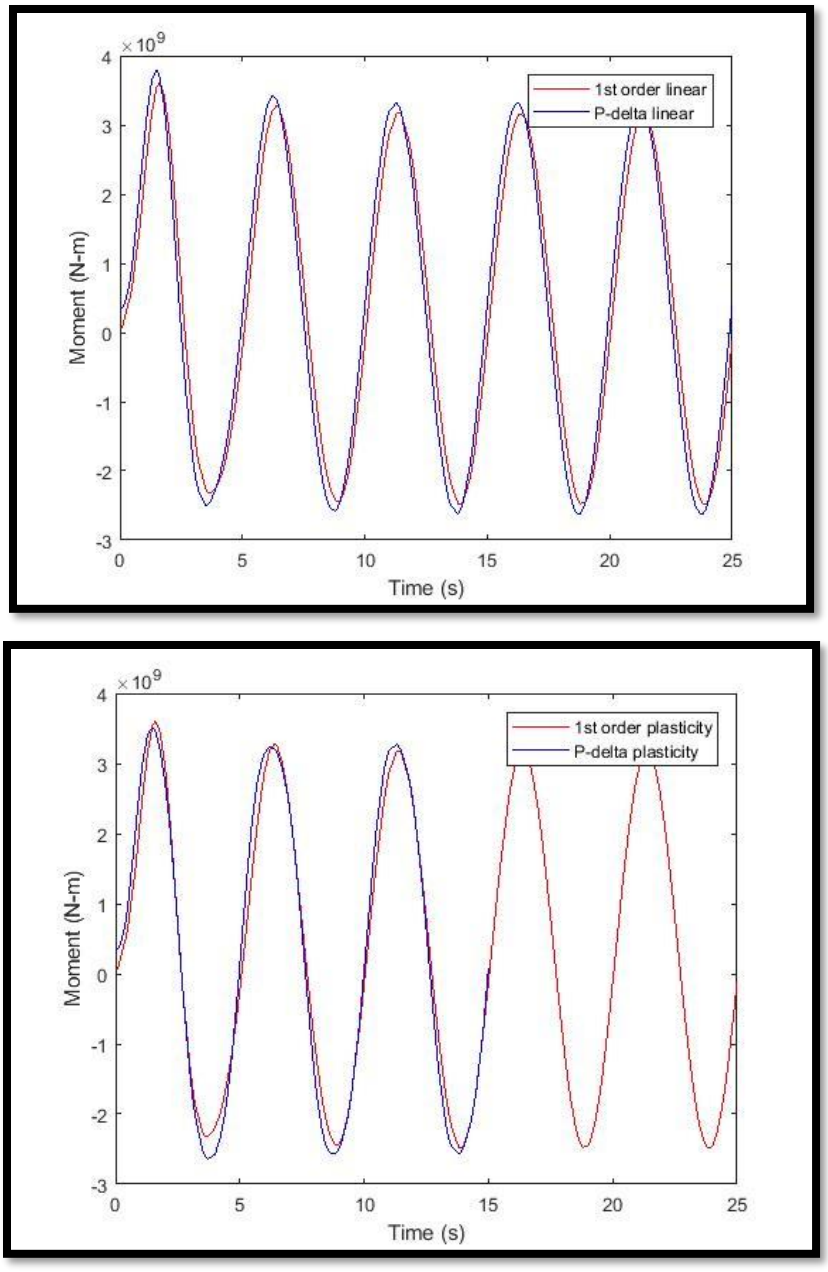

Figure 33: Moment Response Time History, Sinusoidal Motion:20-Story Linear Structure (Top), Nonlinear Structure (Bottom)

The tip displacement time history in Figure 34 for the linear system follows the same trends for low amplification as the 9-story structures with sinusoidal excitation. The nonlinear structure has similar peak values, but the first-order and second-order displacements a slightly phase shifted apart. The phase shifts vary for the different joints in Figure 35, with the largest shift occurring in the middle joints. There is only a small shift in the end joint displacements.

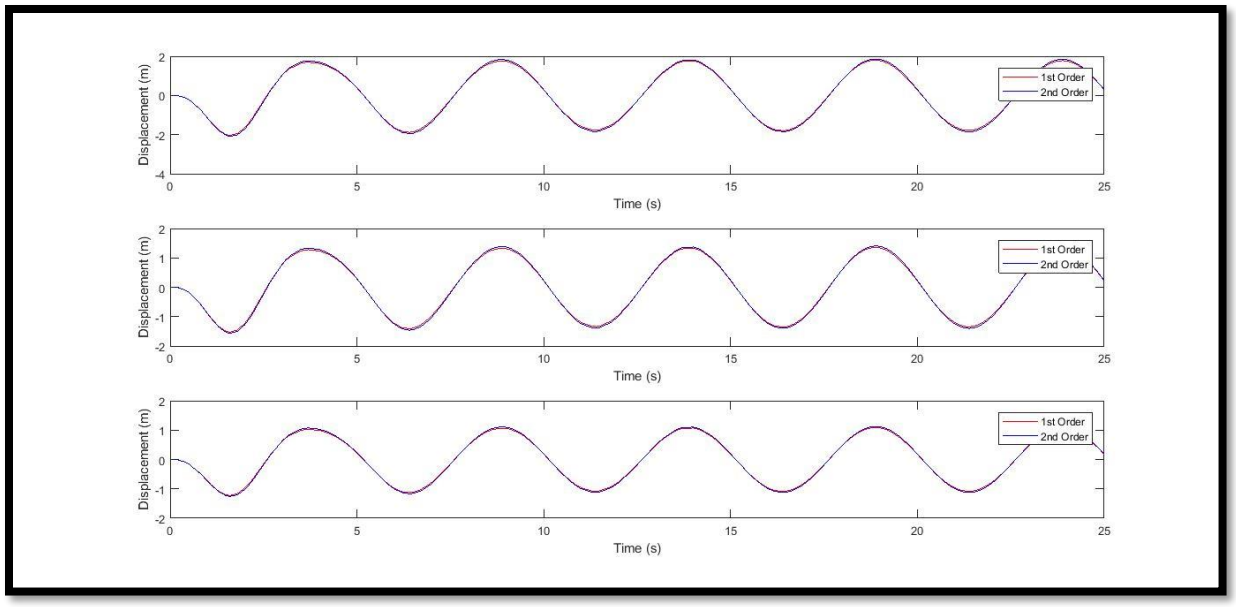

Figure 34: Tip Joint Displacements for 20-Story Linear Structure, Sinusoidal Motion

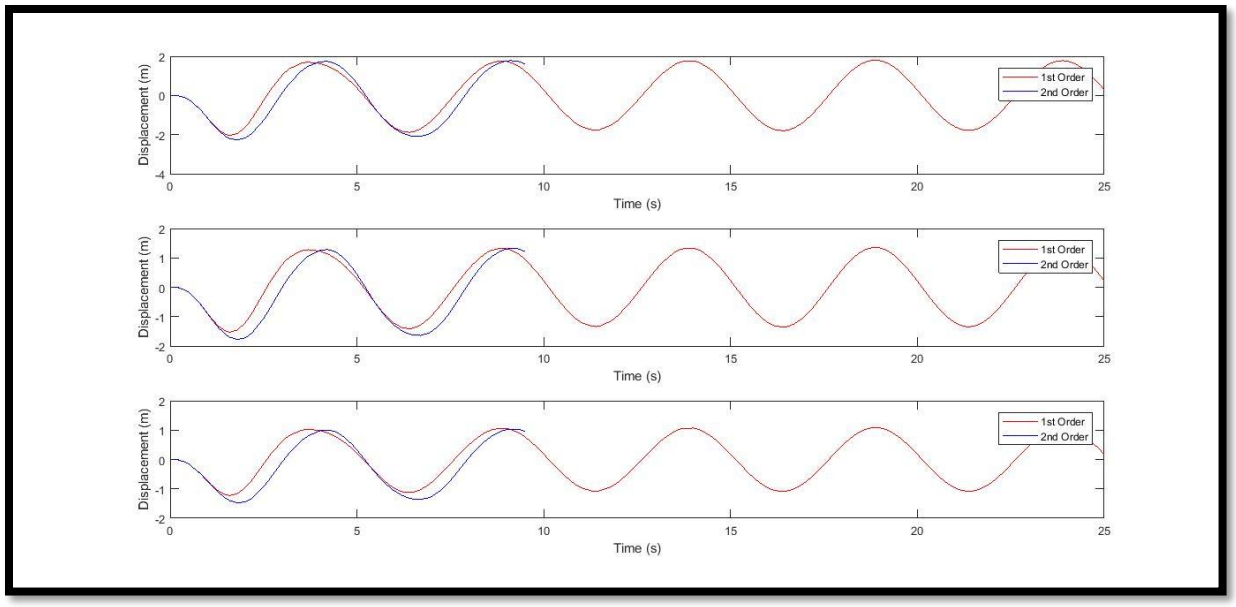

Figure 35: Tip Joint Displacements for 20-Story Nonlinear Structure, Sinusoidal Motion

5.2.2. Kocaeli Ground Motion:

In Figure 36, the first-order and second-order moments follow each other closely for both the linear and nonlinear structures. The moment of the nonlinear structure subjected to second-order analysis stops a time of about 20 seconds. In other scenarios this phenomeon was due to exccessive yielding, but given the low moment values it may be due to some other failure mechanism.

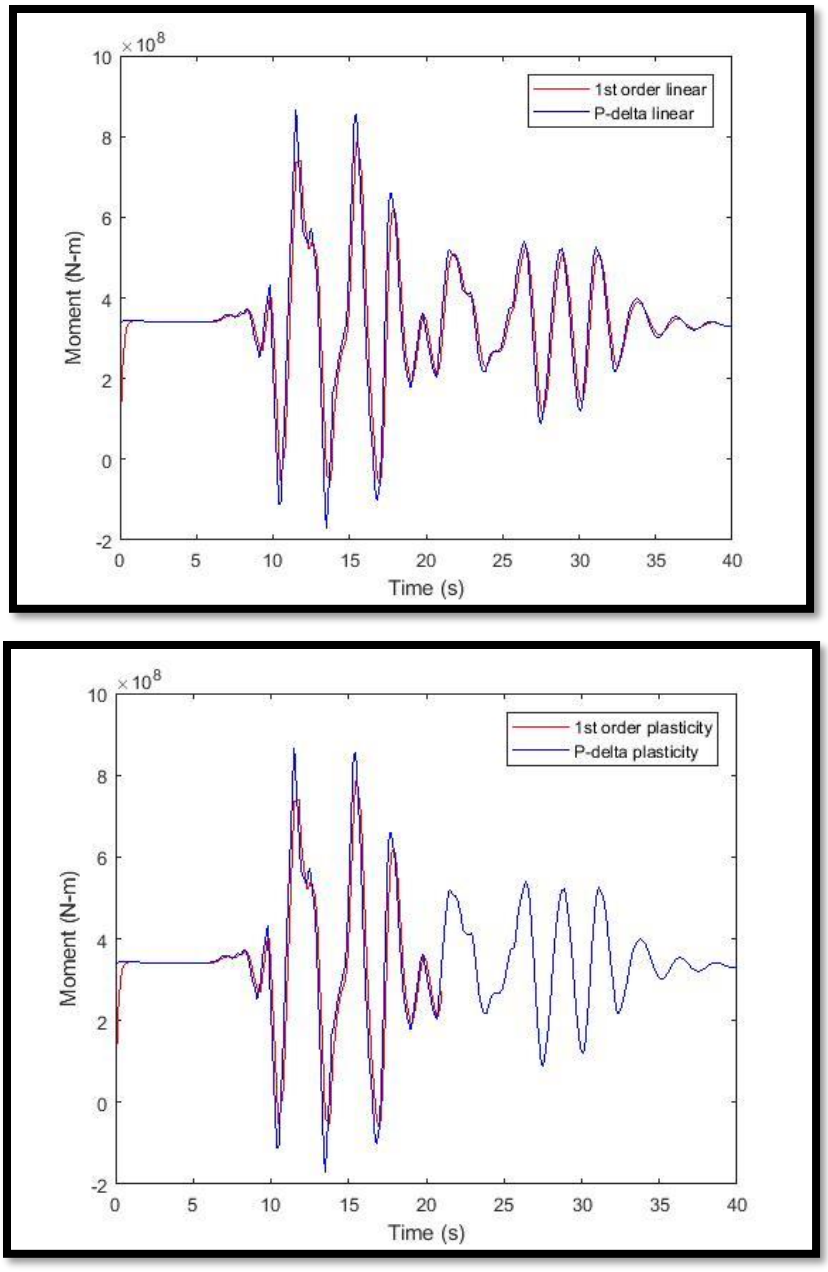

Figure 36: Moment Response Time History, Kocaeli Motion: 20-Story Linear Structure (Top), Nonlinear Structure (Bottom)

The tip displacement time histories for the linear and nonlinear structures show similar behavior and magnitudes of displacements for the first-order and second-order analyses. Unlike the moment time histories, the displacement time histories do not seem to follow the ground excitation, but have local maxima and minima during the most intense portion of ground excitation. In the linear structures, shown in Figure 37, the peak excitation occurs towards the end of the history, between 10 and 20 seconds. The range for the nonlinear structure in Figure 38 is even smaller, between 10 and 15 seconds.

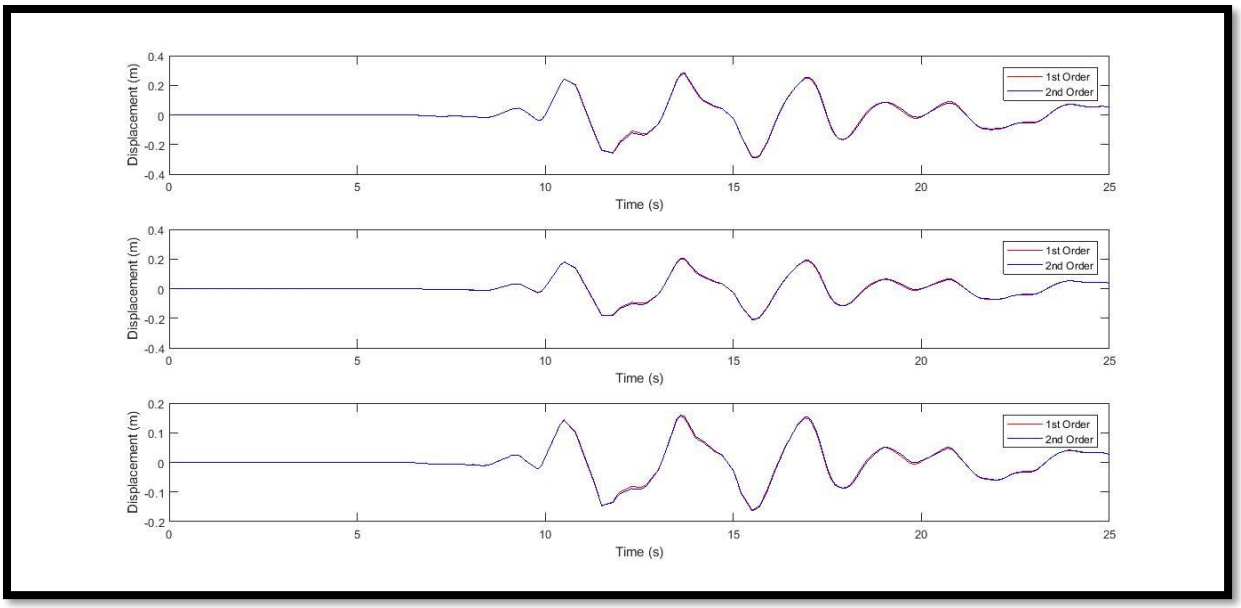

Figure 37: Tip Joint Displacements for 20-Story Linear Structure, Kocaeli Motion

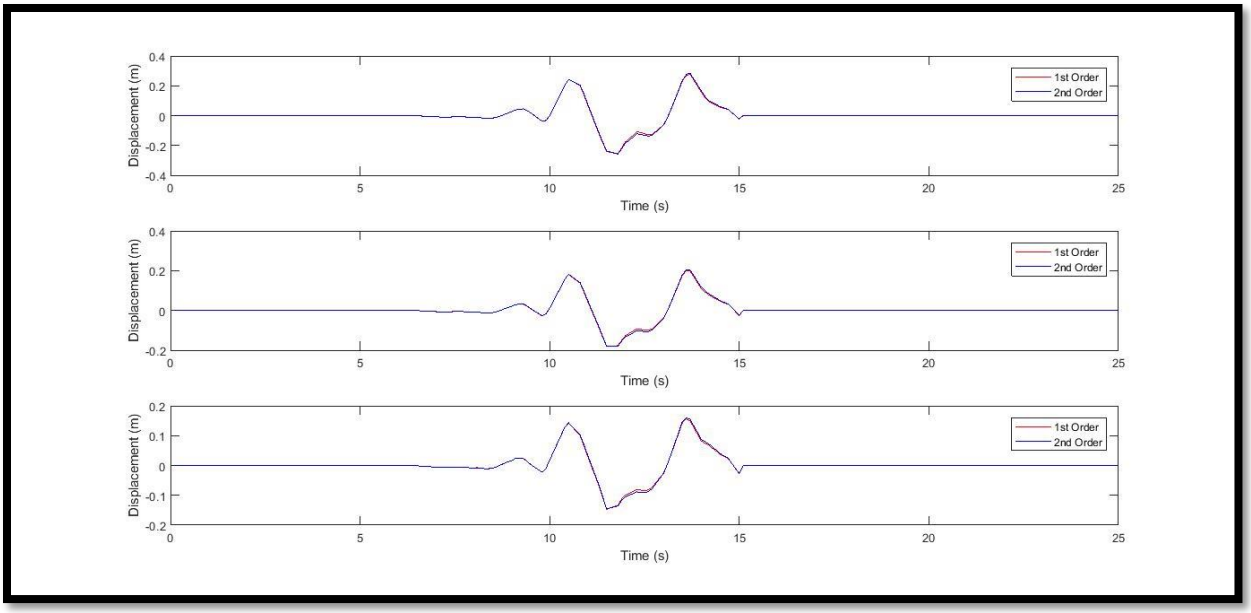

Figure 38: Tip Joint Displacements for 20-Story Nonlinear Structure, Kocaeli Motion

5.2.3. Tohoku Ground Motion:

There was a large change between the first-order and second-order nonlinear structures, shown in Figure 39. In the second-order structure, there are large amounts of plasticity and several member failures.

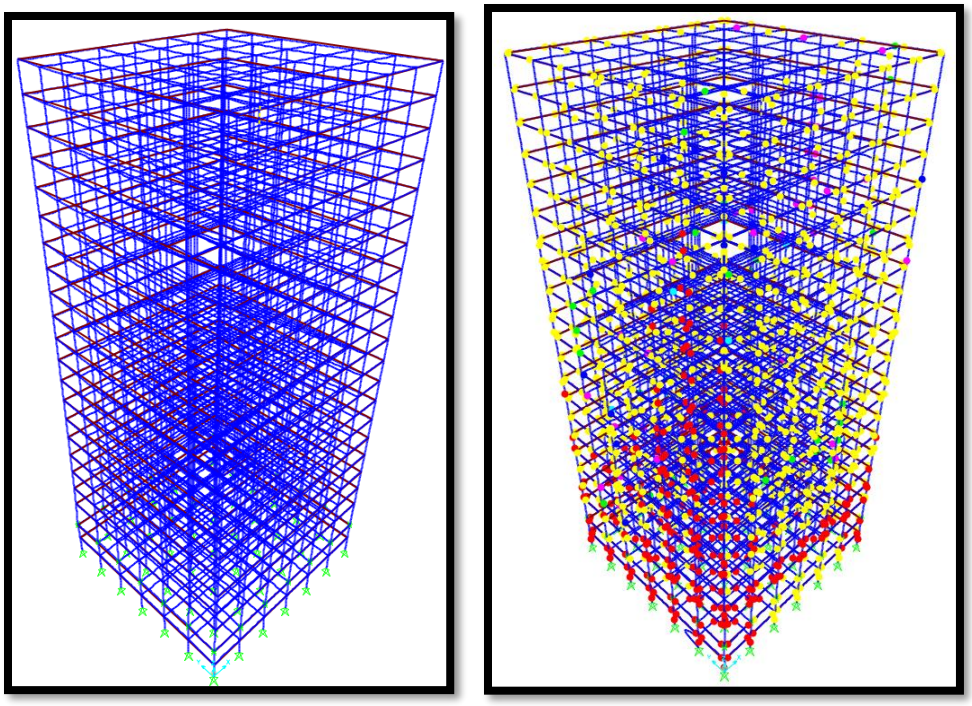

Figure 39: Deformed 20-Story Nonlinear Structure, Tohoku Excitation: First-Order Analysis (left), Second-Order Analysis (right)

The moment fluctuated over time, and the difference between the first-order and second-order data is easily seen, in Figure 40. Each of the moment time histories only extend to a time of about 20 seconds. Some of the data is truncated due to limited computer memory, but it is likely that the second-order nonlinear structure failed before the complete ground motion could be applied.

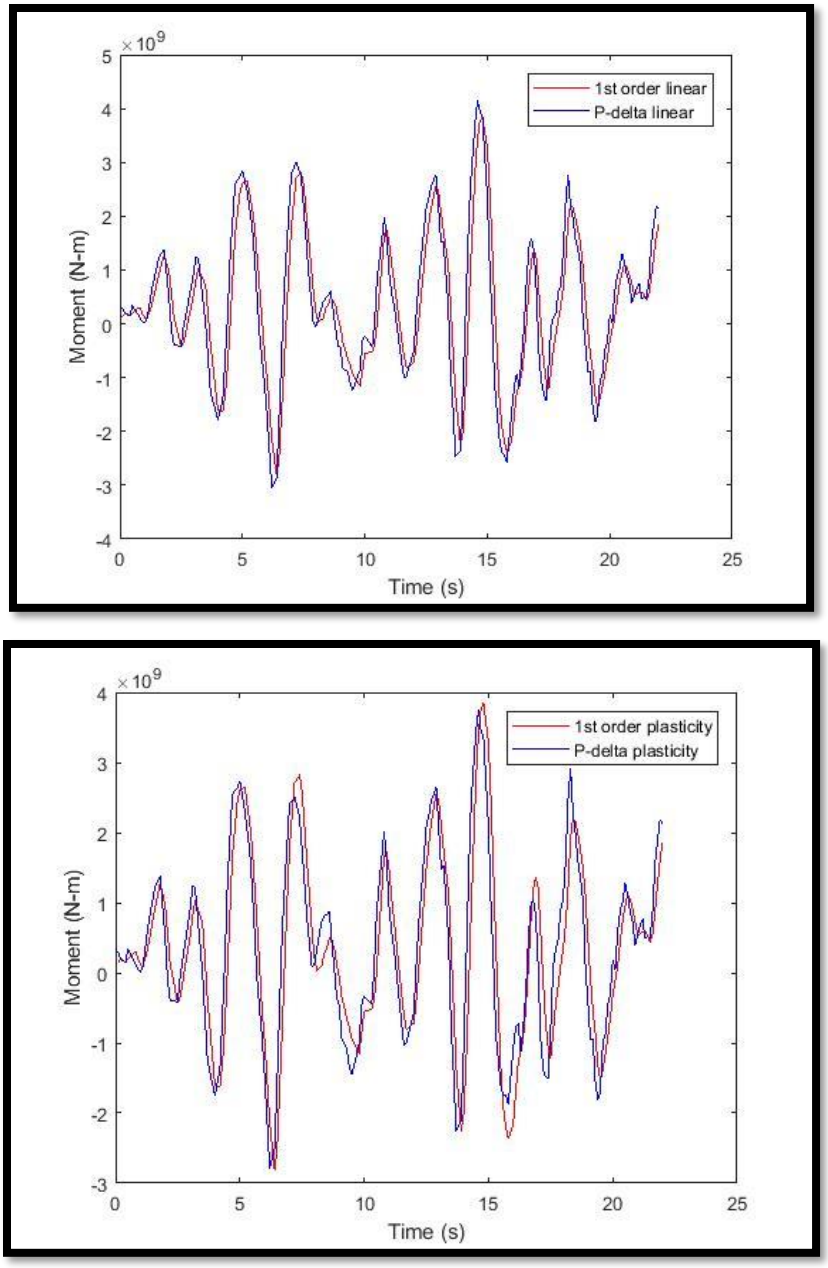

Figure 40: Moment Response Time History, Tohoku Motion: 20-Story Linear Structure (Top), Nonlinear Structure (Bottom)

As with most of the other time history analyses, the first-order and second-order joint displacements have similar values in the linear and nonlinear structures. The linear structure in Figure 41 and the nonlinear structure in Figure 42 have fluctuations throughout the time history that have peaks at the same time regardless of the joint.

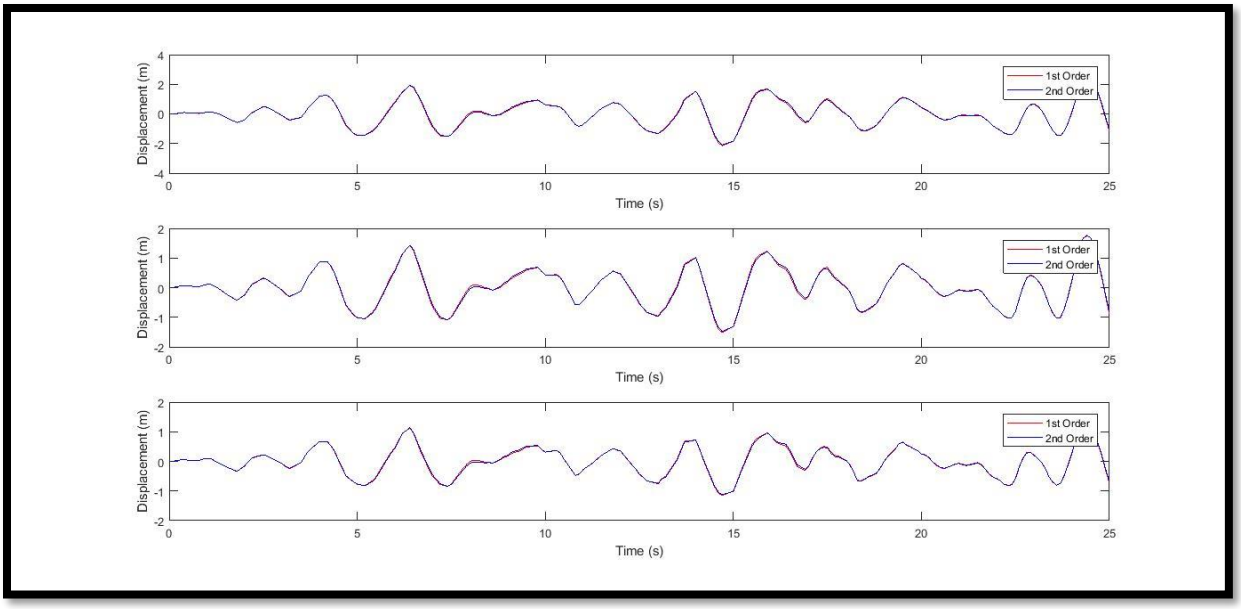

Figure 41: Tip Joint Displacements for 20-Story Linear Structure, Tohoku Motion

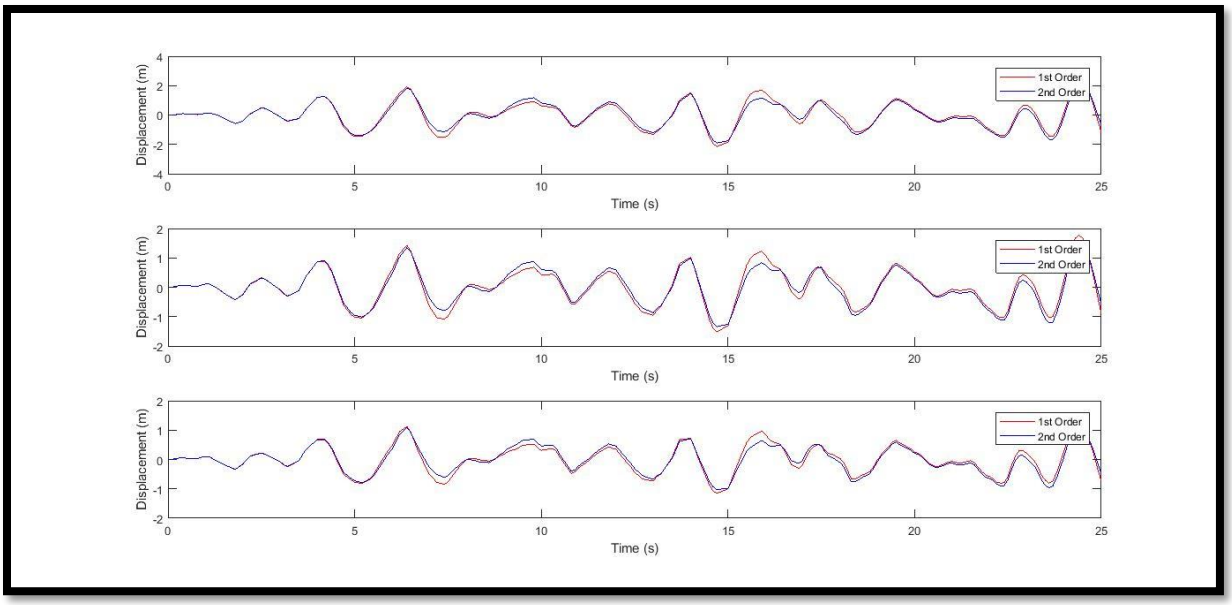

Figure 42: Tip Joint Displacements for 20-Story Nonlinear Structure, Tohoku Motion

5.2.4. Simulated Ground Motion:

In Figure 43 the first-order and second-order moments are close together and continue for the entirety of the time series. The moment has larger peaks towards the end of the time series, suggesting that there is more to the response after 120 seconds.

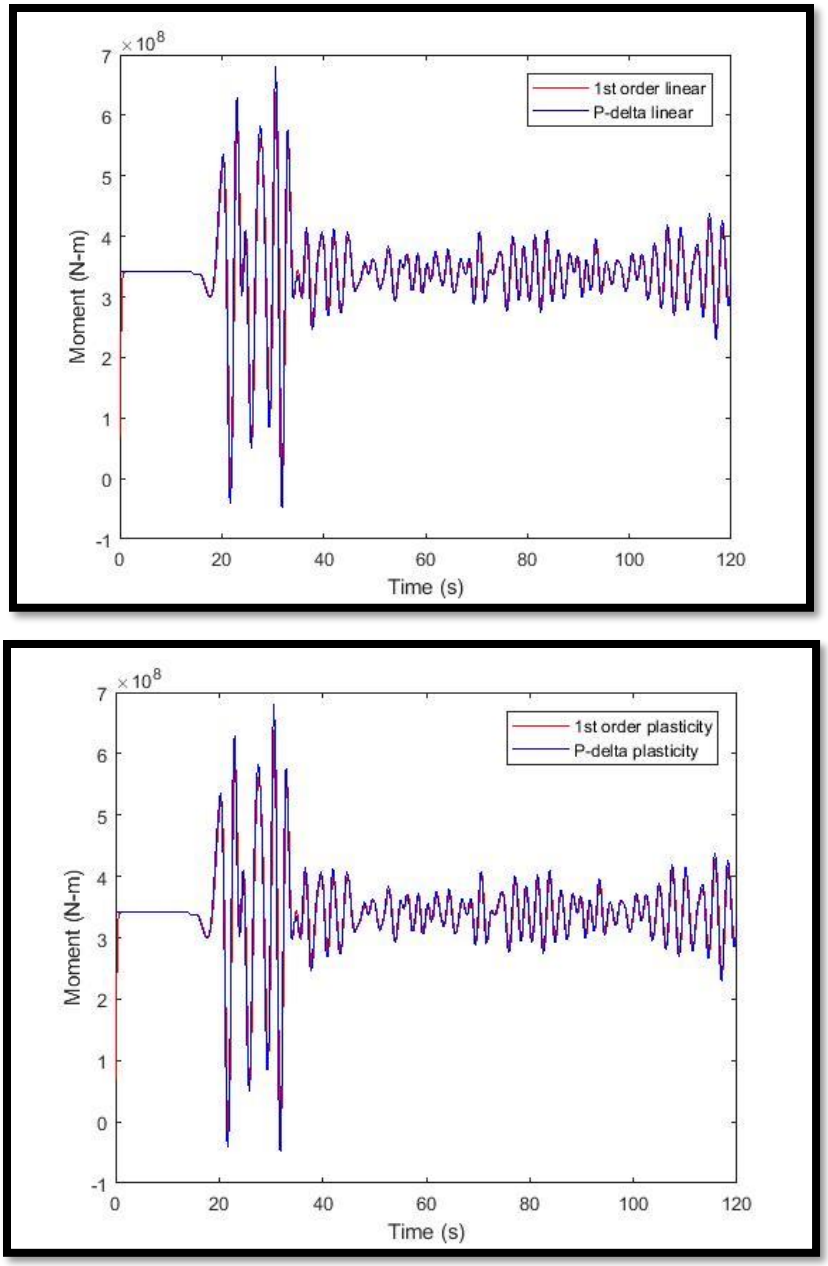

Figure 43: Moment Response Time History, Simulated Motion:20-Story Linear Structure (Top), Nonlinear Structure (Bottom)

The tip displacement time history also suggests that there may be a response past the 120 second end of the ground motion. In both *Figure 44* and *Figure 45* for the linear and nonlinear system, respectively, the displacement is near zero for most of the time. It only reaches its peak at around 21 seconds. The displacement data is limited by the memory issue affecting some of the other datasets.

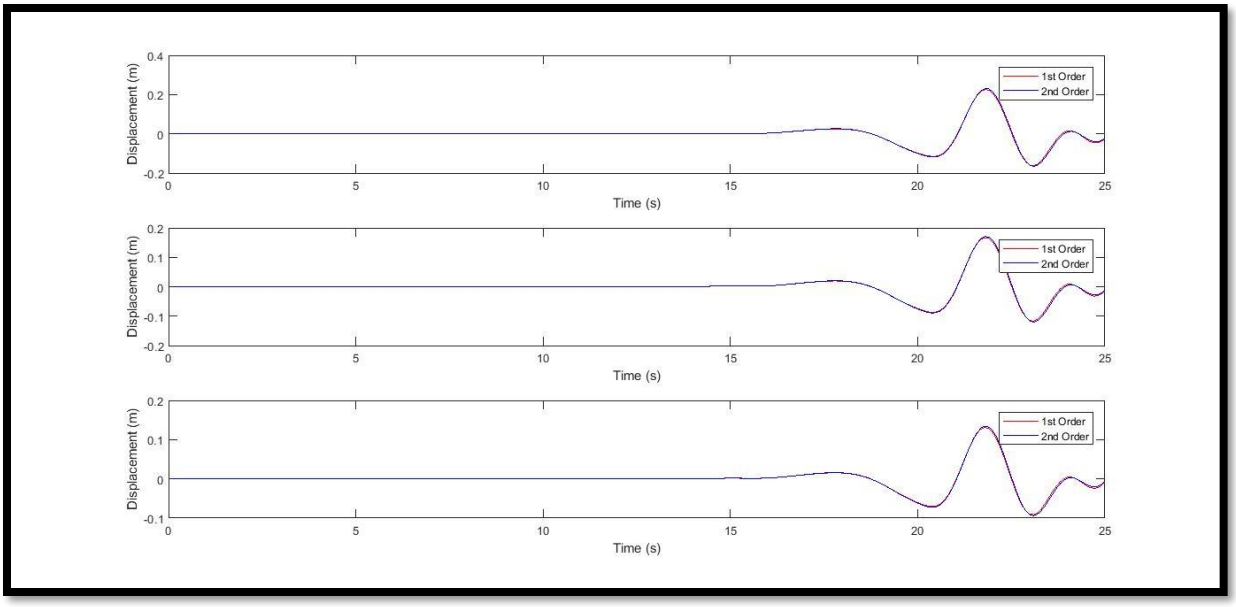

Figure 44: Tip Joint Displacements for 20-Story Linear Structure, Simulated Motion

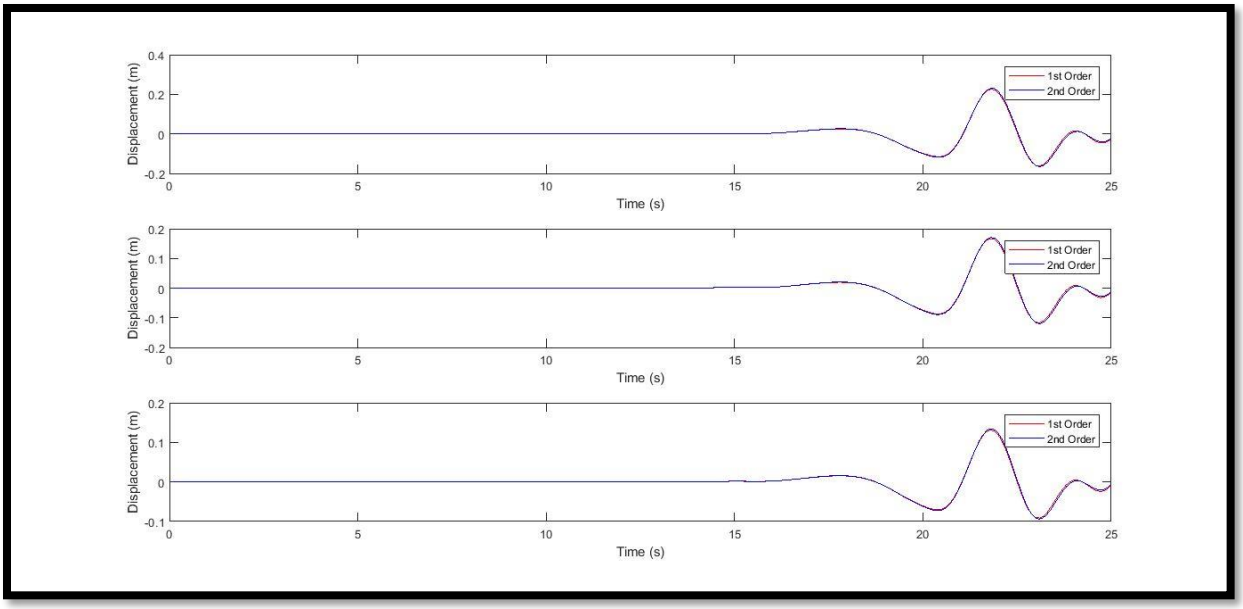

Figure 45: Tip Joint Displacements for 20-Story Nonlinear Structure, Simulated Motion

5.3 Twenty-Story Benchmark Structure: Extended Response

Some of the datasets appeared to have their most intense responses towards the end of the recorded time. In Section 5.2, the end of recorded time was determined by the end of the excitation. In Section 5.3, the recorded time was set as double the length of excitation. This analysis was more limited in comparison to Sections 5.1 and 5.2 due to memory and processing limitations. The Tohoku

data is omitted because it would be a repetition of Section 5.2. Additionally, fewer joints are used in the Simulated ground motion dataset to favor more length-based details over different joints. From Sections 5.1 and 5.2, the trends for tip displacements are reflected across joints and can be extrapolated for Section 5.3. The moment amplification and tip displacement ratios for this extended analysis match those of the shorter-time analysis.

5.3.1. Sine Excitation:

The overturning moment of the structure attenuates quickly after the ground excitation ends. The moment of the first-order nonlinear structure in Figure 46 ends at a nonzero value. The second-order analysis of the nonlinear structure goes to zero as it did in Section 5.2. The moments for the linear structure also reach a nonzero value at the end of the analyzed time. As this linear structure does not account for yielding, there could be some eqivalent force acting on it as a result of the previous ground motion.

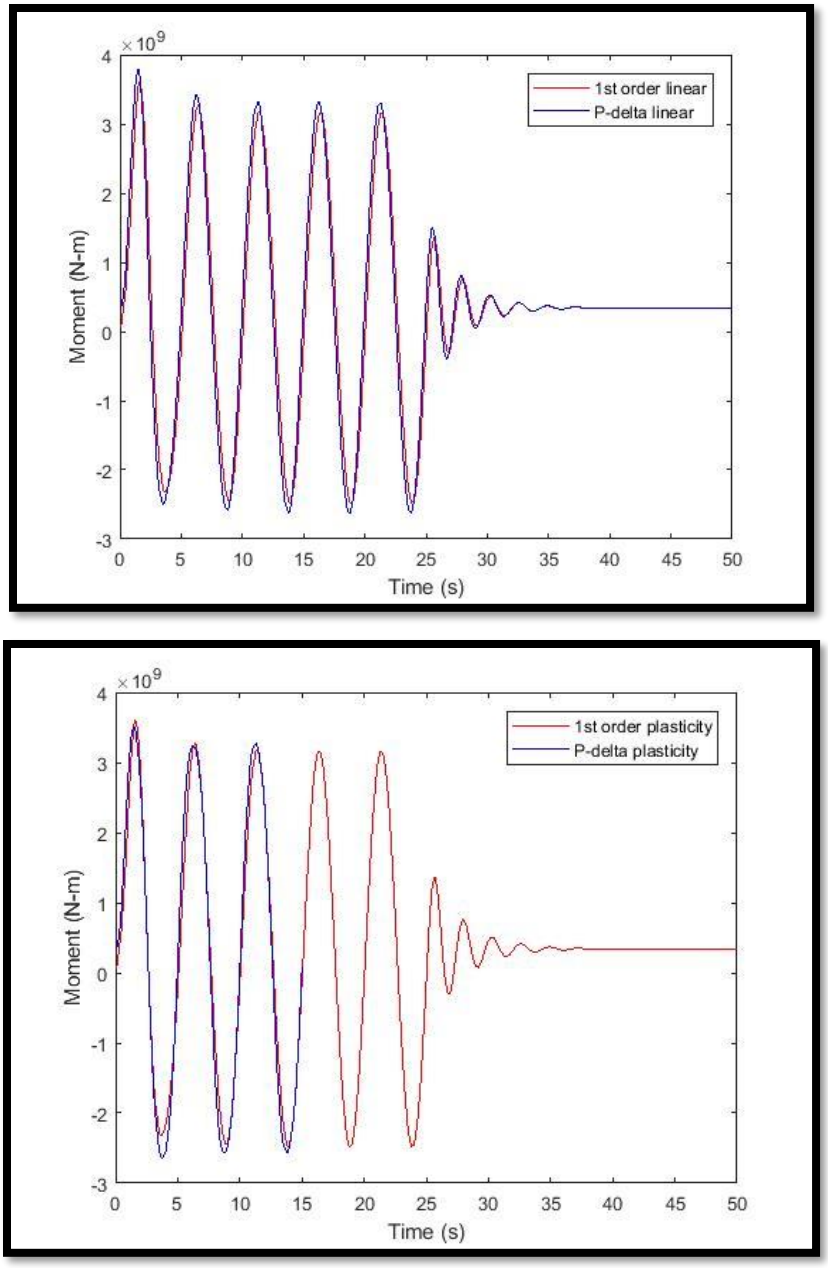

Figure 46: Moment Response Time History, Sinusoidal Motion:20-Story Linear Structure (Top), Nonlinear Structure (Bottom)

5.3.2. Kocaeli Ground Motion:

The moment time history for the Kocaeli acceleration also attenuated quickly and had a similar shape to the analysis in Section 5.2. All of the analyses in Figure 47 had terminating nonzero moment values. This is again likely due to a possible resultant force or yielding action for the linear and nonlinear case, respectively.

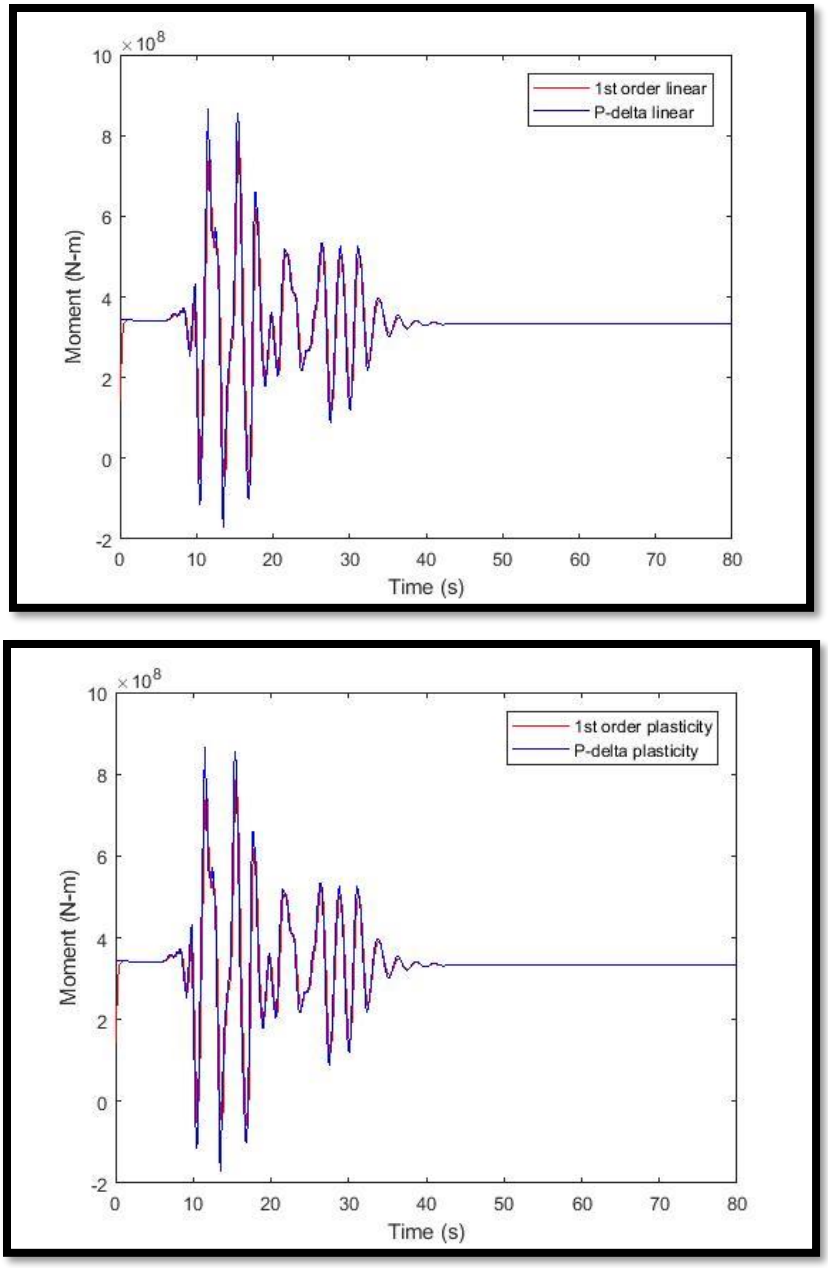

Figure 47: Moment Response Time History, Kocaeli Motion: 20-Story Linear Structure (Top), Nonlinear Structure (Bottom)

5.3.3. Simulated Ground Motion:

The tip displacement time series in Figure 48 does not show much movement past the 120-second end of ground excitation. Only two joints are shown, an exterior and interior joint, due to limited memory and processing power. In the interior joint in both the linear and nonlinear structure,

the first-order displacement shows activity towards the end of the analyzed time. This may indicate partial resonance for one of the mode shapes.

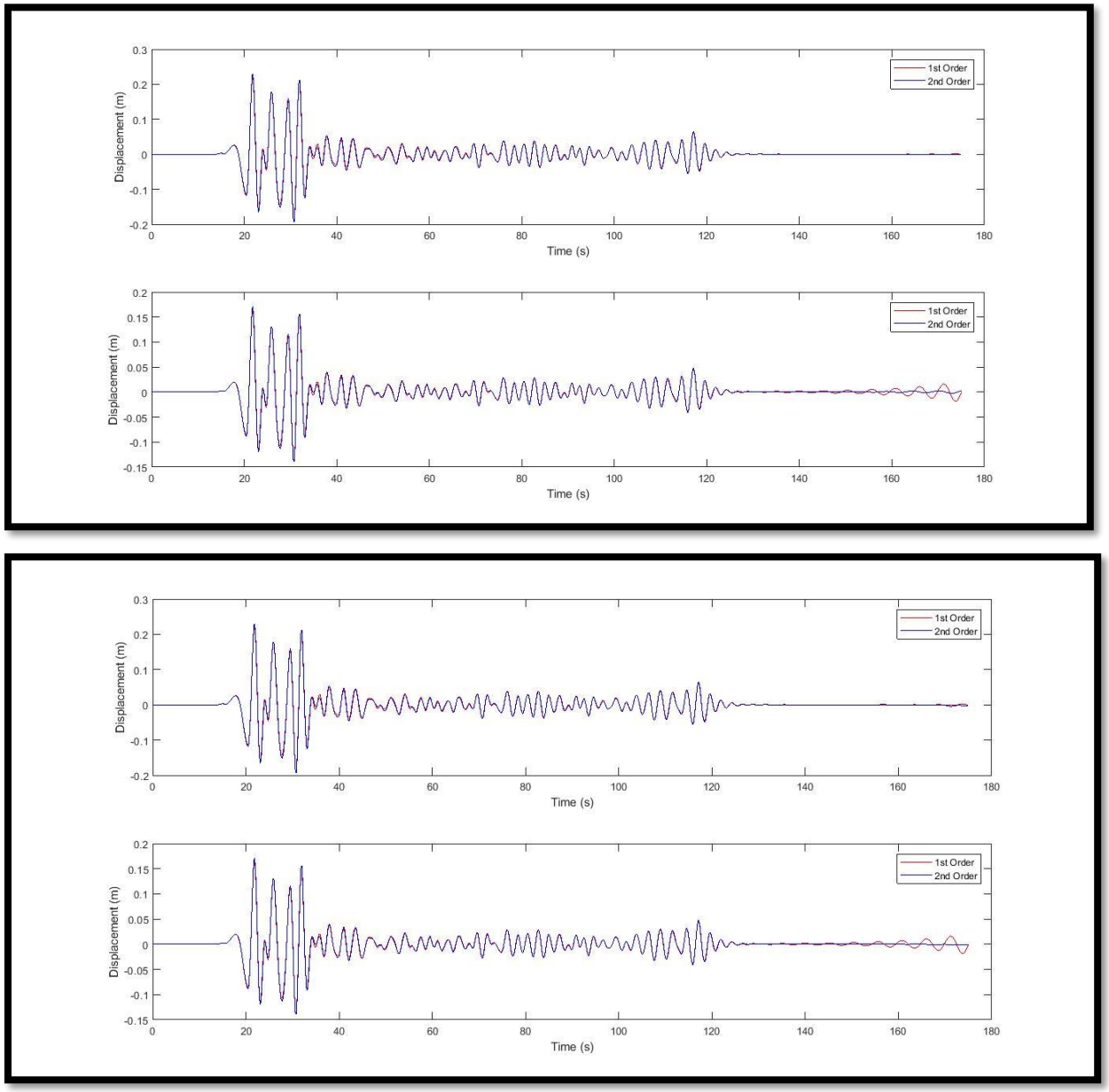

Figure 48: Tip Joint Displacements for 20-Story Linear (Top) and Nonlinear (Bottom) Structure, Simulated Motion

CHAPTER 6. CONCLUSIONS

High-intensity ground motion can cause large moments and displacements on structures depending on the characteristics of the motion, which can be amplified slightly by including second-order analysis. The amplification of the moments and displacements due to the second-order effects does not seem to be a significant amount for the ground motions analyzed in this paper. The moment amplifications were usually below 10%, while the displacement amplifications were usually below 5%.

Although the amplifications are low, a second-order analysis should not be neglected, especially in nonlinear structures. Especially in the 20-story nonlinear structures, the addition of second-order effects resulted in more members yielding for some ground excitations. The ground excitations played a major factor in the structure's response, and it is important to consider several ground motions for the structure's analysis as required by ASCE7.

REFERENCES

Aagaard, B., Brocher, T., Dolenc, D, Dreger, D., Graves, R., Harmsen, S., Hartzell, S., Larsen, S., McCandless, K., Nilsson, S., Petersson, N., Rodgers, A., Sjögreen, B., and Zoback, M. (2008). "Ground Motion Modeling of the 1906 San Francisco Earthquake, Part II: Ground-Motion Estimates for the 1906 Earthquake and Scenario Events." *Bulletin of the Seismological Society of America,* 98(2), 1012-1046.

American Society of Civil Engineers (ASCE). (2017). *ASCE 7-16: Minimum Design Loads and Associated Criteria for Buildings and Other Structures.* Chapter 16.

Computers and Structures Inc. (CSI). (2018). "SAP2000 Integrated Software for Structural Analysis and Design." (20)

Eads, L. (2012). "Pushover Analysis of 2-Story Moment Frame." *Open System for Earthquake Engineering Simulation - Home Page*, (Nov. 17, 2018).

Olsen, A., Aagaard, B., and Heaton, T. (2008). "Long-Period Building Response to Earthquakes in the San Francisco Bay Area." *Bulletin of the Seismological Society of America*, 98(2), 1047-1065.

Ohtori, Y., Christenson, R., Spencer, B., and Dyke, S. (2004). "Benchmark Control Problem for Seismically Excited Nonlinear Buildings." *Journal of Engineering Mechanics*, 130(4), 366-385.

Pacific Earthquake Engineering Research Center (PEER). (2014). "NGA-West2." *PEER Ground Motion Database*, (Nov. 17, 2018).

Seismosoft (2016). "Seismosignal."

Senzen, H., and Whittaker, A. (2006). "Seismic Performance of Industrial Facilities Affected by the 1999 Turkey Earthquake." *Journal of Performance of Constructed Facilities*, 20(1), 28-36.

Song, S., Beroza, G., and Segall, P. (2008). "A Unified Source Model for the 1906 San Francisco Earthquake." *Bulletin of the Seismologic Society of America*, 98(2)

Srinivasu, A., and Rao, P. (2013). "Non-Linear Static Analysis of Multi-Storied Building." *International Journal of Engineering Trends and Technology*, 4(10), 4629–4633.

Tsai, V., Bowden, D., Kanamori, H. (2017). "Explaining extreme ground motion in Osaka basin during the 2011 Tohoku earthquake." *Geophysics Research Letter*, 44, 7239-7244.